Laboratory studies on air-hydrate crystals

Tsutomu Uchida* and Takeo Hondoh**

*Hokkaido National Industrial Research Institute, AIST, MITI, Tsukisamu Higashi 2-17, Sapporo 062-0052, JAPAN
**Institute of Low Temperature Science, Hokkaido University, N19W8, Sapporo 060-0819, JAPAN

Abstract: Experimental studies on air-hydrate crystals from both ice cores and those grown in the laboratory are reviewed to summarize the present knowledge of their properties, nucleation, growth, and dissociation. The physical properties of air-hydrate crystals have been determined mainly through spectroscopic techniques. The main objective of these studies is determining the type and number of air molecules located in the hydrate cages. The formation and growth processes of air hydrates have been studied directly by observing them embedded in ice crystals. But, because formation and growth is too slow to study in laboratory, knowledge of the diffusion of gas molecules through both ice and hydrate are needed to understand hydrates in ice cores. Lastly, we discuss the stability conditions and the dissociation process of air hydrates to predict the optimal storage conditions of ice cores without their serious damages.

1. Introduction

At the surface of an ice sheet, snowfalls transform into a firn layer. In this layer, atmospheric gases can migrate through the free space in the firn. However, as the firn layer is compressed from continuing snowfalls, the firn changes to ice and traps some of the atmosphere in air bubbles. This builds up a record of the atmospheric air and water along the depth axis in the ice sheet. Thus, we can obtain the time variation of gas content in the air and isotopic compositions of water molecules by the analysis of deep ice cores.

Air bubbles are stored atmospheric gases in the shallow parts of ice sheets. They are observed to shrink due to the increase of hydrostatic pressure with depth. Because these air bubbles contain pressurized gas, they can cause the ice to fracture during ice drilling. But this "fracture zone" is limited to the depth region with high-pressure bubbles; at depths less than a few hundred meters, the pressure is too low, and deeper than approximately 1000 meters the bubbles do not exist. The location of the air molecules that were once in bubbles was initially unknown. It was first thought that they were distributed in the ice crystals. This was because the total amount of gases in the clear deep ice was nearly that in the bubbly ice near the surface. However, because the solubility of gas molecules in ice is very

Physics of Ice Core Records
Edited by T. Hondoh
Hokkaido University Press, 2000, Sapporo

small, the location of the air was still a mystery.

Miller [1] proposed an answer to this mystery in 1969. Based on the phase equilibrium of ice and gas mixtures, he suggested that clathrate hydrates, i.e., air hydrates, formed from compressed bubbles in the polar ice sheet. The air-hydrate formation occurs when the pressure in the bubble P_b is greater than the dissociation pressure P_d, which is determined as the following function of the bubble air composition and the transformation process temperature T

$$P_d = X_{N2} P_{N2} + X_{O2} P_{O2} . \quad (1)$$

The original paper [1] assumed that X_{N2} and X_{O2} were the nitrogen and oxygen mole fractions in the gas phase, respectively, and their sum was approximately unity. However, these values should be replaced by those in the hydrate phase, X_{N2}^H and X_{O2}^H, respectively [2, 4]. P_{N2} and P_{O2} are the dissociation pressures of pure nitrogen and oxygen, respectively, expressed in MPa as

$$log\, P_{N2} = 3.6905 - 688.9 / T \quad (2\text{-}1)$$

$$log\, P_{O2} = 3.679 - 717 / T . \quad (2\text{-}2)$$

As described in section 4.1, X_{N2}^H and X_{O2}^H are determined by X_{N2}, X_{O2}, and the gas pressures. Thus, we can estimate the ice depth that air bubbles can transform to air hydrates.

Hydrate inclusions in ice were first discovered by Shoji and Langway [3] in 1982. They found transparent inclusions in deep ice cores recovered from Dye3 in Greenland and confirmed that the inclusions were air hydrates. Since the solubility of gas molecules in an ice is very small, the ancient atmospheric gases included in the deep ice sheet are stored in air hydrates (Fig. 1).

The formation of air-hydrates affects several important aspects of ice core analysis. First, air-hydrate crystals store the "real" air molecules of paleo-atmospheres. Their small volume is offset by their large gas concentration: approximately 170 times denser than that at standard temperature and pressure [4]. Second, the formation of air hydrates eliminate the ice fracture during ice core drilling. This is because the high-pressure gases become relatively immobile in their solid-state hydrates. Third, gas capturing in this solid-state form can also reduce the driving force on gas diffusion through the ice matrix. This is important for the time resolution of gas composition in the deeper parts of the ice sheet because the resolution depends both on the annual layer thickness and on the gas diffusion rate beyond the annual layer. In addition, the transition of air bubbles to air hydrates increases the transparency of ice. This phenomenon is a key issue for observing decay events during a neutrino observation project in a deep hole in the ice (AMANDA project) [5].

Analyses of air-hydrate crystals in ice cores have recently attracted attention as a way to understand the paleo-climate. One type of ice core analysis is to understand the distribution of air hydrates in deep ice cores. Shoji and Langway [6] used a microscope to study air hydrate crystals at their shallowest depths from several deep ice cores. From the comparison of them with the distribution with the predicted phase diagram of air hydrates, they found that the phase diagram was satisfactory for predicting the transformation depth of air-bubbles to air hydrates.

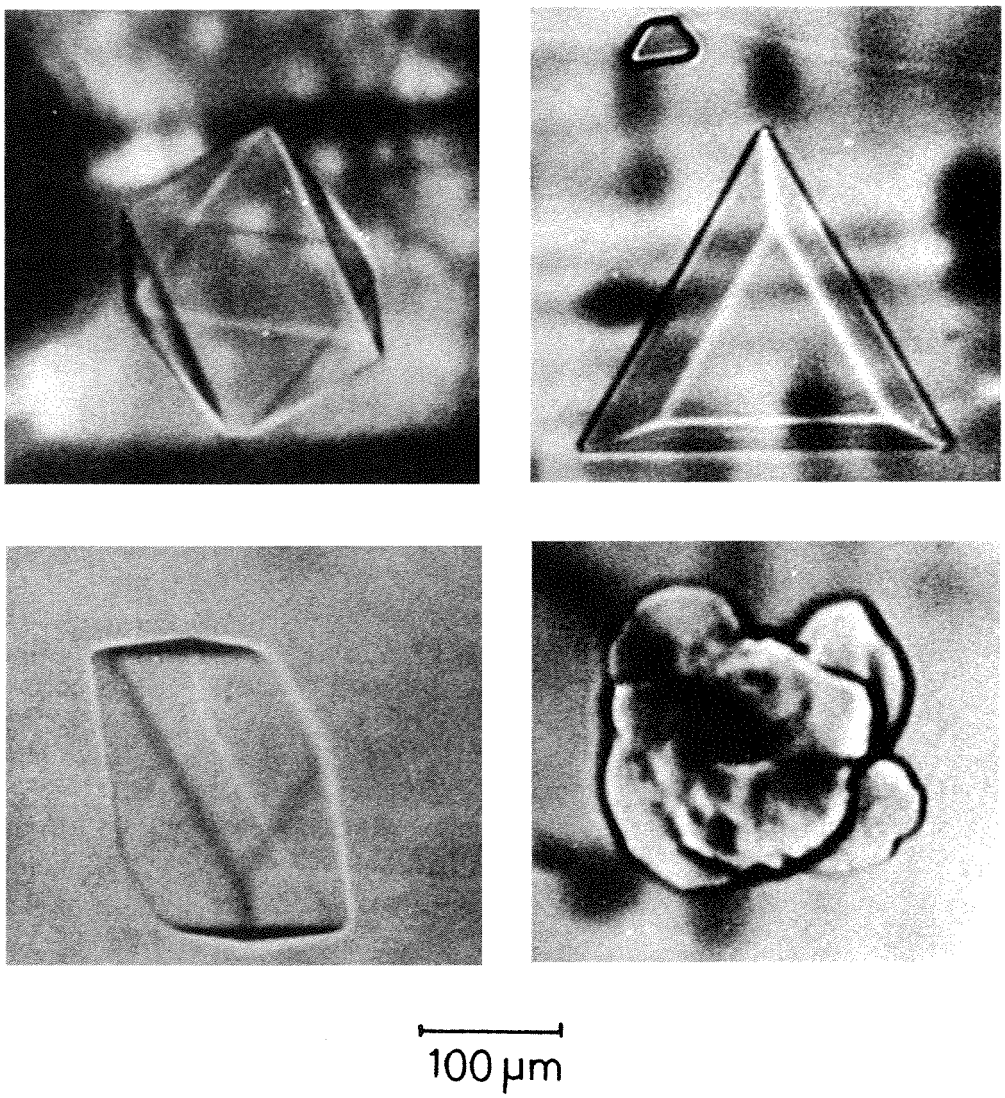

Figure 1: Various air hydrates observed in an ice core from Dye-3, Greenland (From Nakahara et al. [23]).

Uchida et al. [7] found that the number density of air hydrates versus depth accurately correlated with climatic temperatures. As shown in Fig. 2, a large number of small crystals of the hydrates were included in cold periods while a small number of large crystals formed in warm periods. Since air hydrates are transformed from air bubbles, the air-hydrate distribution should be attributed by that of air bubbles. The air-bubble distribution is known to be affected by the surface temperature of the ice sheet because smaller snow crystals in the lower temperature makes smaller air spaces in the firn. Therefore it is concluded that the size

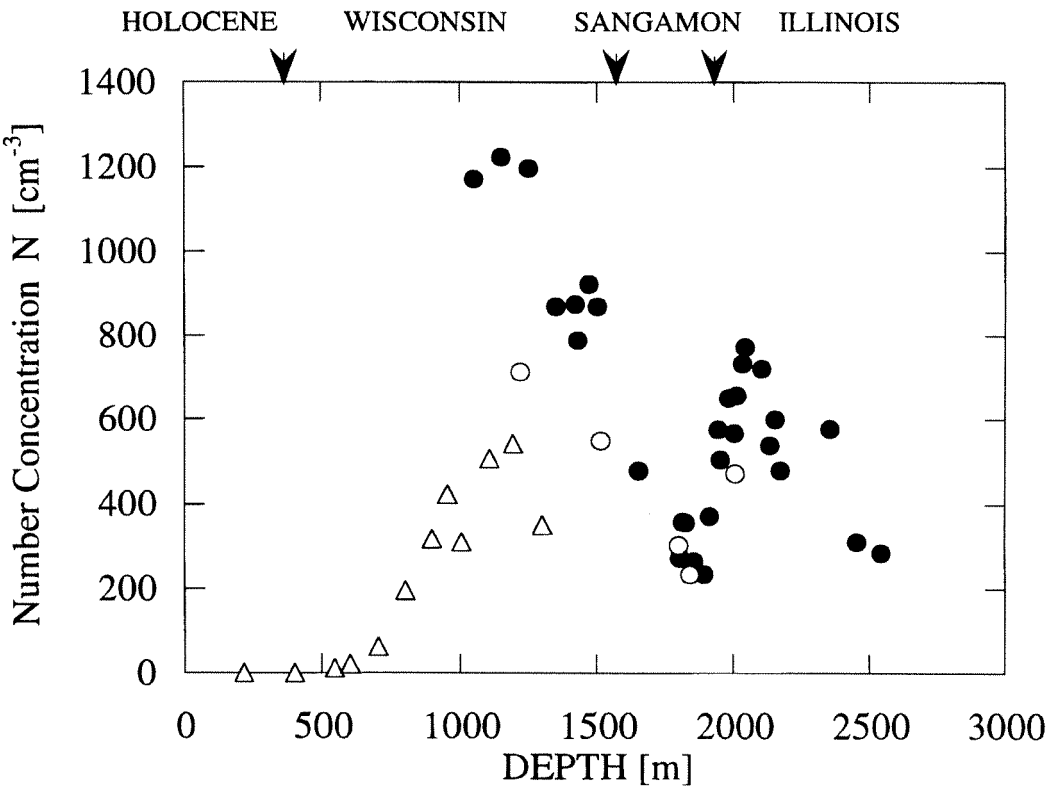

Figure 2: Depth variation of the number concentration of air hydrates in Vostok ice cores (modified for ref. 7). A large number of small crystals of hydrate were included in cold periods (Wisconsin and Illinois) while a small number of large crystals in warm periods (Sangamon). Three series of ice cores were used (solid circles, open triangles, and open circles).

distribution mainly depends on the surface temperature of the ice sheet. Thus this size distribution can be used to check if the isotope data is giving a clear picture of past climates. Detailed information on this is in another review by Lipenkov [8].

Although it is important, obtaining the depth distribution of such small and transparent inclusions in ice is difficult because the microscopic observations must be done under severe experimental conditions. New techniques have been developed that involve laser scattering tomography [9] partially alleviate this problem.

Most of the paleo-climatic information derived from ice core analyses are related to the physical properties, the formation and growth processes, and the stability conditions of air-hydrate crystals in ice cores. Many studies have been done to clarify the nature and structure of these natural clathrate hydrates. Furthermore, laboratory studies on air-hydrate crystals are indispensable for understanding the formation and growth processes of the crystals and their interaction with the surrounding ice matrix.

This review is primarily about laboratory studies of air-hydrate crystals

and is organized as follows: In section 2, we review the physical properties of air-hydrate crystals as deduced from ice core analysis. The measurement techniques were mostly X-ray diffraction, Raman spectroscopy, and interferometric observations. The crystallographic investigations are required to understand the paleo-atmospheric conditions, such as the gas composition and the fraction of clathrate cages that are occupied by gas molecules. The latter is called the cage occupancy. Recently, computer simulation studies have been used to understand the physical properties of air hydrates with greater detail, but assuming certain molecular interactions. They help to improve our understanding of physical property analyses. The mechanical properties of air-hydrate crystals are also important for interpreting the depth distribution of air-hydrate crystals related to the ice flow.

Section 3 is a review of the formation and growth processes of air-hydrate crystals in an ice matrix. The formation of air-hydrates from air bubbles was directly observed in the laboratory. This dynamic process was found to be very fast compared to the glacial time-scale. On the other hand, the growth process of air-hydrates involves the diffusion of gas molecules through an ice matrix. Therefore, we review some gas diffusion measurements in ice. Kuhs et al. [10] has a review of the formation and growth of air hydrates, and Ikeda et al. [11] describes details of gas diffusion through an ice matrix in their review.

The final section, section 4, is a review of air-hydrate dissociation and its stability conditions. This process must be considered for the handling of ice core samples without causing significant changes. The results from a few relevant experiments are discussed and used to estimate the optimal storage environment for ice cores.

2. Crystallographic structures of air hydrates

Crystallographic analyses are very important for interpreting ice core data related to air-hydrate crystals. The air-hydrate clathrate is a crystal compound with a cage structure formed by water molecules (host lattice) and includes individual air molecules (guest molecules) in the molecular cages. Physical properties of the hydrates can come from properties of the host lattice, the guest molecule, or the interactions between guest and host molecules. Furthermore, the physical properties of ice including air hydrates may be affected by that of air-hydrate crystals.

In this section, we describe crystallographic analysis of air hydrates. Spectroscopic measurements, such as X-ray diffraction and Raman spectroscopy, are the most common techniques in crystallography of air hydrates. In section 2.1 and 2.2, we discuss X-ray diffraction and Raman spectroscopic studies on air-hydrate crystals that indicate properties of both the host lattice and guest molecules. Recently, computer simulation has become a powerful tool to understand molecular-scale properties. Simulation studies that can be compared to spectroscopic measurements are reviewed in section 2.3. Based on the crystallographic analysis, studies on the cage occupancy in air hydrate crystals are reviewed in section 2.4. Mechanical properties are discussed in section 2.5.

2.1 Crystallographic analyses by X-ray diffraction

Some of the questions that these studies can answer are, what is the structure of air hydrate crystals that are transformed from air bubbles included in hexagonal ice crystals, and how are air molecules confined in the hydrate crystals. Also, it is important to know the crystallographic structure of air hydrates to understand the crystal growth process and to understand the interactions between air hydrates and ice crystals.

X-ray diffraction is the best way to determine crystal structures. However, special techniques are required when using air hydrate crystals because they have a high dissociation pressure. Using equations (1) and (2), pure air hydrate crystals are not stable at atmospheric pressure with temperatures above 147 K. Therefore, a 1-mm cube of ice with a hydrate crystal at the center was prepared from ice cores and used as the sample [12].

Hondoh et al. [13] showed that natural air-hydrates in polar ice cores (Dye-3, 1500-m deep) are cubic even though the structure of ice crystal is hexagonal. Moreover, the crystallographic structure was also determined to be Stackelberg's structure II clathrate hydrate [12, 13]. Before this finding, the crystallographic structure of air hydrates was thought to be structure I [14]. The finding that guest molecules smaller than methane will form the structure II clathrate hydrate had also been reported for Ar-hydrates in a neutron diffraction study [15]. Now, the crystal structure of gas hydrates which have guest molecules smaller than methane is known to be structure II [16]. It is thought that such small guest molecules are more suitable for forming the 12-hedral cages (small cage) and structure II has more small cages than structure I [16, 17].

Because most of the natural-air-hydrate samples were single crystals (as determined by their facets), precise structure analysis by X-ray diffractometry on the crystal of also indicated the distribution of guest molecules encaged in the clathrate structure. X-ray diffraction usually measures only the host lattice, but detailed measurements allowed us to obtain the guest information in cages because the interaction between guest molecules and the host lattice causes some deviations in the measurements. This analysis indicated occupation by air molecules in both types of cages [12, 13]. Fig. 3 shows the distribution of air molecules in the cages using electronic density cross-sections through the centers of the (a) 12-hedron, and (b) 16-hedron cages. The contours are every 0.02 $e \cdot A^{-3}$ interval. This figure shows that air molecules in the small cages are centered in the cage, whereas the air molecules are too small to remain in the center of the larger, 16-hedron cage. The location of the guest molecules in the 16-hedron cage are considered to be determined by the same distance from the wall of the cage, which is similar to the guest-host distance in the 12-hedron cage. Based on a thermodynamic model [18], the interaction between guest molecules and the host lattice is van der Waals. Therefore, this interaction is thought to largely determine the crystal structure.

Neutron scattering measurements [19, 20] indicated the location of N_2 molecules in both small and large cages of laboratory-grown N_2 hydrates. The best model to fit the experimental data had the N_2 molecule at the small-cage center and the N_2 molecule shifted from the center of the

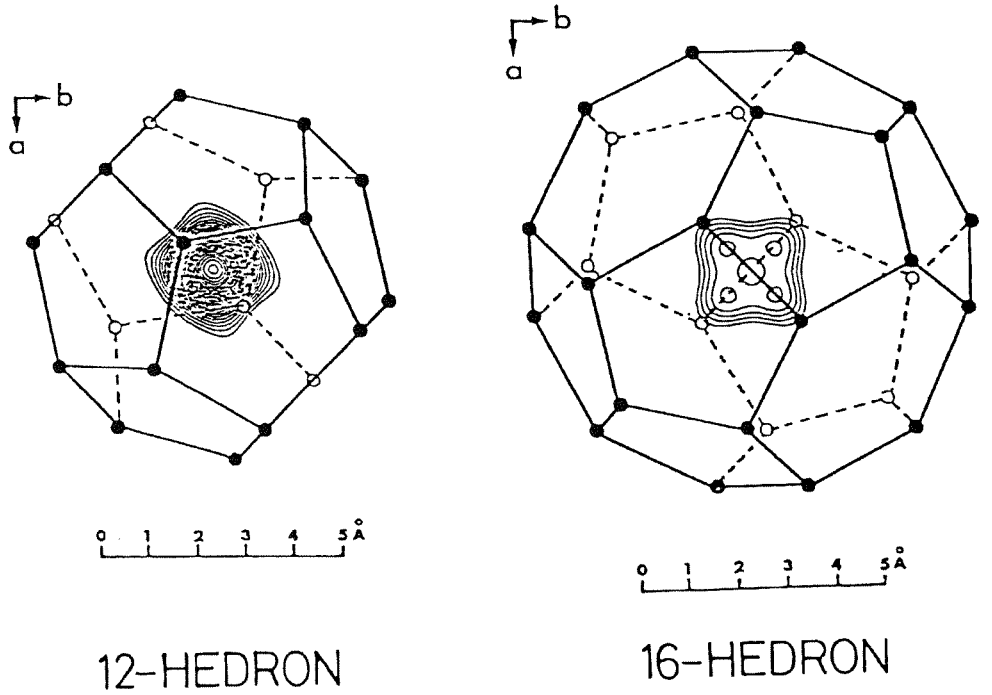

Figure 3: Distribution of air molecules in the cages. Electron density cross-sections through the center of the cages: (a) 12-hedron, (b) 16-hedron. Contours at 0.02 $e \cdot A^{-3}$ intervals. This figure shows that air molecules in small cages remain close to the center of the cage, whereas air molecules are too small to remain at the center of the large (16-hedron) cage. (From Hondoh et al. [13].)

large cage by approximately 0.8 Å. These results coincided with those obtained by X-ray diffraction measurements on natural air hydrate crystals.

The thermal properties of air hydrates are useful for predicting how the hydrates change with temperature, such as the relaxation of ice cores during the sample storage. Linear thermal expansion of air hydrates was inferred by the temperature dependence of the lattice constant of air-hydrate crystals as measured by X-ray diffraction [21]. The resulting linear thermal expansion of air-hydrate crystals is 4.4×10^{-5} K^{-1} at 273 K. (This value can also be used to calculate the density of hydrate crystals at a given temperature.) This value is nearly the same as the ice matrix (5.6×10^{-5} K^{-1}) and THF clathrate hydrate [22] (5.0×10^{-5} K^{-1}) at the same temperature. (THF is a structure II hydrate.) Because air hydrate crystals are included in the ice matrix during the experiment, the obtained value might have been brought closer to that of ice. However, the same order of the linear thermal expansion of air hydrates with that of the isolated THF hydrate, which also has structure II, suggests that the obtained value for air hydrates in ice is intrinsic and was not affected by the surrounding ice matrix. More work on this issue is needed.

2.2 Guest molecule measurements in air hydrates by Raman spectroscopy

When the small transparent inclusions were first discovered in the deep ice cores, they were identified as air hydrates because a large amount of gas was released from the inclusions during their decomposition. At the time they were simply labeled air-hydrates. But it was not known if there were separate crystals of nitrogen (N_2) hydrate and oxygen (O_2) hydrate in the ice. It was also not known how guest molecules are included in cages. To answer these questions, spectroscopic analysis has advantages. Since air hydrates must be analyzed with ice matrix, as in the X-ray diffraction measurements, infrared spectroscopy is not practical because of absorption by the ice. Therefore, Raman spectroscopic measurements have been applied to analyze the air hydrate crystals in ice core samples.

The first crystallographic analysis by Raman spectroscopy on natural air-hydrates (see Fig. 1) used the Dye-3 ice cores from Greenland [23]. From measurements of their molecular vibrations, the major guest molecules in the crystals were identified as nitrogen and oxygen. Each spectrum was shifted to lower wave numbers from that of the vapor phase. This indicates that the motions of guest molecules in cages are slightly restricted by the host lattice.

Hence, the Raman spectroscopic analysis [23] showed that the air hydrate crystal was the mixed gas hydrate of N_2 and O_2. The ratio of the N_2 intensity to the O_2 intensity in the hydrate, the N_2/O_2 ratio, indicated that the gas composition in air hydrates was approximately twice as O_2-rich as that of the present air. This was called the "missing nitrogen problem". One suggested explanation of this phenomenon was N_2 gas escape during ice core storage because N_2 hydrate has a larger dissociation pressure than O_2 hydrate.

Recently, precise Raman spectroscopic analyses have been carried out [11, 24–27] to measure the depth distribution of the N_2/O_2 ratio. However, there were no O_2-rich hydrates in GRIP ice cores, Greenland, from well below the transition zone to the deepest part of the ice sheet [26, 27].

Ikeda et al. [24] carefully measured the Raman spectra of air hydrates, considering this crystallographic anomaly. They found that condensation of mostly oxygen occurred only in the transition zone from air bubbles to air hydrates. In this zone, the "missing nitrogen" was found to be in the remaining air bubbles. They explained this peculiar phenomena by diffusive migration of N_2 and O_2 from air bubbles to air hydrates. This molecular process is driven by higher concentration of gas molecules dissolved in ice matrix of air bubble surfaces than those at ice-hydrate interface, and the fractionation is caused by faster migration of O_2 and N_2. The intensity ratio of N_2 and O_2 were nearly that of the present air in the depth regions where only air bubbles or air hydrates existed. A more detailed treatment of this, including the fractionation process between N_2 and O_2, is in Ikeda et al. [11]. This result explained also the difference found in the degree of fractionation between the Antarctic and the Greenland ice cores.

Ikeda et al. [28] showed that the Raman intensities of both guest and host molecules varied with the crystal orientation using polarized Raman spectroscopy. The Raman intensity variation of guest molecules was caused by restricted rotations of the guest molecules due to the cage structure. This result supports the measured Raman spectrum

shifts of both guest molecules to lower wave numbers than those from the vapor phase. This crystallographic anisotropy was taken into consideration for the method to determine the N_2/O_2 ratios described above.

2.3 Computer simulation studies on air hydrates

The above mentioned measurements require molecular-level knowledge of hydrates to fully interpret the results. A useful tool for this interpretation is computer simulations. For instance, molecular dynamic (MD) calculations have been done to study hydrate stability [29–32]. Tabata et al. [33] studied the stability of argon hydrate by using an MD simulation that included the intermolecular KKY potential [34]. Their application of this model to air hydrate properties allowed more detailed spectroscopic analysis on air hydrate crystals.

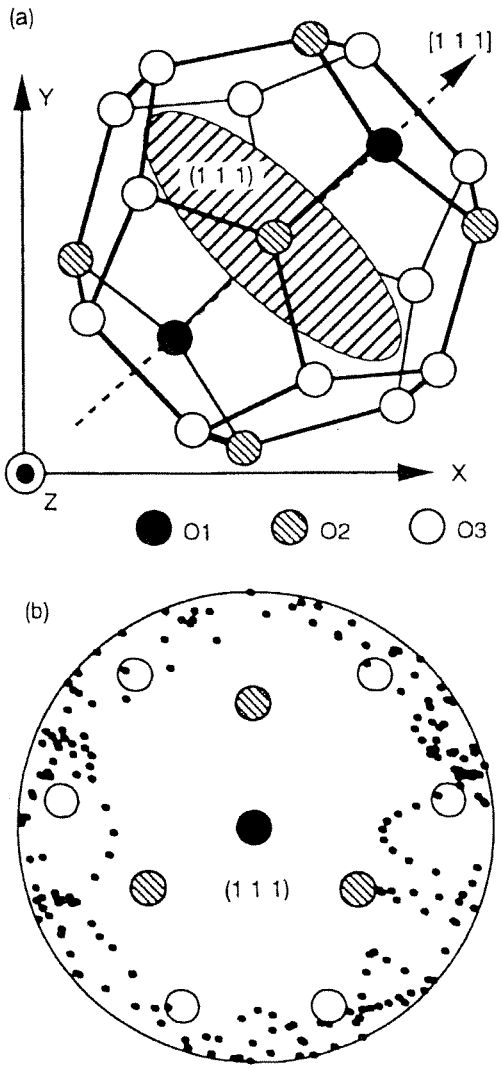

Figure 4: Stereographic projection of nitrogen molecule orientations in a small cage at 50 K. Oxygen atoms of host water molecules, designed O1, O2 and O3, form the 12-hedral small cage. The dashed arrow in Fig. 4a (denoted as [111]) indicates the compressed axis of the small cage, which corresponds to the axis normal to the page and located at the center of Fig. 4b. (From Horikawa et al. [35].)

Horikawa et al. [35] simulated the Raman intensity of both nitrogen and oxygen for different crystallographic orientations. They found that the change of the relative Raman intensity resulted from restricted molecular rotations caused by the cage configurations. The detailed description is as follows: Air molecules occupy both types of cages of structure II, as shown in Fig. 3. Although air molecules in the large cages can rotate relatively freely, those in the small cages are slightly restricted because the free radius of the small cage nearly equals the van der Waals radius of air molecules [4]. Furthermore, both nitrogen and oxygen are linear, not spherical molecules, so there is a preferred rotation axis. Fig. 4 shows the stereographic projection of molecular orientations of nitrogen in a small cage at 50 K. Oxygen atoms of host water molecules, labeled O1, O2, and O3, form the small cage which is slightly compressed in the O1-O1 (or [111]) direction. The projection (Fig. 4b) indicates that the diatomic guest molecules preferably lie on the (111) plane, the normal of which corresponds to the O1-O1 direction. This simulation agrees with the experimental results [28].

2.4 Studies of cage occupancy of air hydrates

In section 2.1, we described the crystallographic structure of air hydrates. The result indicates that the density of the host lattice is approximately 0.795 g·cm^{-3} at 273.2 K, which is calculated by the lattice parameter obtained from X-ray diffraction [21]. This value is smaller than that of ice. Then the density of air hydrates depends on the (total) cage occupancy of the guest molecules and its composition. Fig. 5 shows the calculated density of air-hydrate crystals for different cage occupancies and of gas compositions. In the same figure, the density of ice is indicated by an arrow and the host lattice density for the structure II hydrate is shown at the point of zero cage occupancy for each line (approximately 0.795 g·cm^{-3}).

The low cage occupancy is related to the large amount of defects (vacancies) which might affect a hydrate's stability and mechanical properties. As shown by MD simulations, the cage occupancy is important for the stability of gas hydrates. Furthermore, these vacant cages may play an important role in hydrate growth and the diffusion of gas molecules through the hydrate crystal; that is, they allow the diffusion of guest and host molecules through the hydrate (see section 3).

Estimated cage occupancies of air hydrate crystals are also used to estimate the gas concentration in ice core samples. The total gas content, which is an indicator of the ice sheet thickness [36], is closely related to the total volume of air hydrates and their cage occupancy because most atmospheric gas molecules in deep ice sheets should be stored in air hydrates. Therefore, measurements of cage occupancy are identified as one of the basic core analyses.

The theoretical cage occupancy of gas hydrates can be estimated by the following equation [18]:

$$\Delta\mu_w = -kT\,[ln(1-\theta_L)/17 + 2\,ln(1-\theta_S)/17]\,, \tag{3}$$

where $\Delta\mu_w$ is the chemical potential difference between the hydrate lattice and ice, and θ_L and θ_S are the occupancies of large and small cages, respectively. The equilibrium cage occupancy of N_2 hydrate

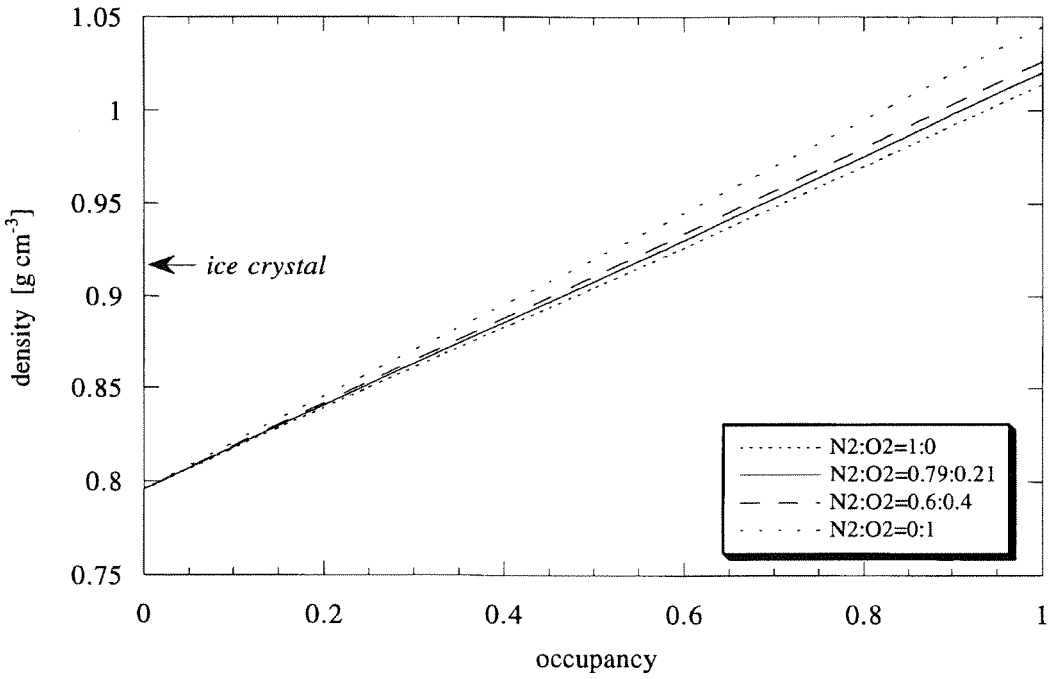

Figure 5: Calculated density of air hydrate crystals. Each line has a different gas composition shown in the legend. The lattice parameter is assumed to be 17.0 A and the molecular weights of water, nitrogen, and oxygen are 18.025 g, 28.013 g, and 31.999 g, respectively [57].

[10] at 273 K and 30 MPa is approximately 0.86 assuming the parameters proposed by Parrish and Prausnitz [37]. This value is considered as the recommended occupancy because the hydrate is in equilibrium with enough gas [18].

The cage occupancy estimated from the neutron scattering data, assuming the two-constant, solid-solution model, was approximately 0.89 (0.85 for small cage and 0.97 for large cage) [19, 20]. Since the air hydrate is transformed from an air bubble in which the initial gas volume was fixed, the cage occupancy of natural air hydrates could differ from the theoretical values. Measuring the cage occupancy of air hydrates in ice core is still in its infancy.

Parameter fitting of the X-ray diffraction data [12, 13] from natural air hydrates with the theoretical structure model revealed that the cage occupancy in both cages were approximately 0.8. (The large cage occupancy ranged from 0.6 to 1.0 and the small one from 0.7 to 0.8.) This was the first direct measurement of the cage occupancy of air hydrates; it showed that the cage occupancy was not unity and varied with the samples. However, it is very difficult to determine precisely using only X-ray diffraction data. Several techniques are required to accurately determine the cage occupancy of air-hydrate crystals.

In situ neutron diffraction is another method to obtain the precise crystallography of hydrates. Kuhs et al. [19, 20] measured the cage occupancy for both small and large cages of laboratory-grown nitrogen hydrates as well as their lattice constants. They found agreement between the measured and theoretical cage

occupancies at pressures lower than approximately 30 MPa. Above 30 MPa, double cage occupancy of nitrogen molecules in the large cage of structure II was discovered. This is consistent with the four population-maxima of air molecules in the large cage of structure II, which was obtained from X-ray diffraction analysis [12, 13] (see Fig. 3). This might occur in the deepest part of an ice sheet. More details of this are summarized in Kuhs et al. [10].

The refractive index is a useful parameter for estimating the cage occupancy ratio of air-hydrate crystals [38]. Based on the Onsager cavity model [39], the refractive index of air hydrates should vary with the air composition and cage occupancy. Observations with a microscope suggested that the refractive index of air hydrates is slightly larger than that of ice [3]. This small difference in refractive

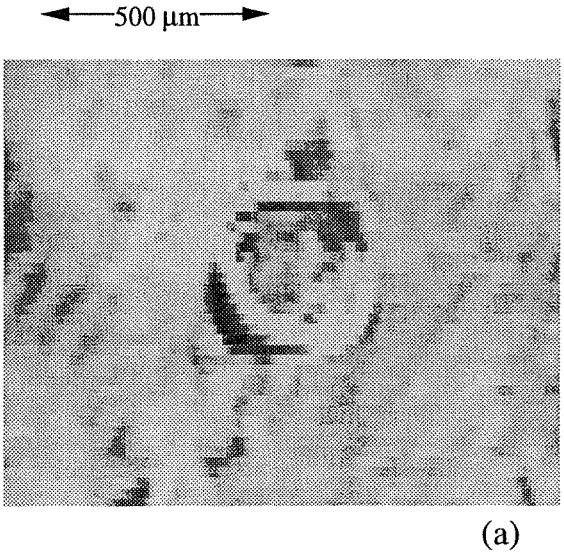

Figure 6: Images of an air-hydrate crystal with (a) schlieren system (sharpen the boundary between ice and hydrate) and (b) Mach-Zehnder interferometer (the relative shift in the fringe is proportional to the difference in refractive indices and crystal thickness). (From Uchida et al. [38].)

indices was one reason that air hydrate crystals were not discovered in ice cores right away. To determine such small differences of refractive indices, an interferometric measurement is useful. Fig. 6 shows the images of an air-hydrate crystal with (a) a schlieren system, and (b) a Mach-Zehnder interferometer. They measured the refractive index of air-hydrate crystals in 2542-m deep Vostok ice cores, Antarctica, relative to that surrounding ice crystal. It was 1.3137(16) assuming the refractive index of the surrounding ice crystal was 1.3084(7) [38]. Fig. 7 shows the calculated refractive index with the parameters of both air composition and cage occupancy. From this value, the density and the cage occupancy is 1.047 $g \cdot cm^{-3}$ and approximately 0.93, respectively assuming the air composition is $N_2 : O_2 = 0.79 : 0.21$.

Uchida et al. [7] estimated the cage occupancy from the total volume of air hydrates and the total gas content. The result agreed with the cage occupancy estimated from the refractive index measurements. Use of the relations between air hydrate volume, cage occupancy, and the total gas content showed that most of ancient air had been stored in air hydrates, not in the ice matrix. The comparison of air hydrate volume and total gas content also indicated the possibility of a depth dependence of the cage occupancy (Fig. 8).

2.5 Mechanical properties of air hydrates

The mechanical properties of air hydrates also have applications to ice-core

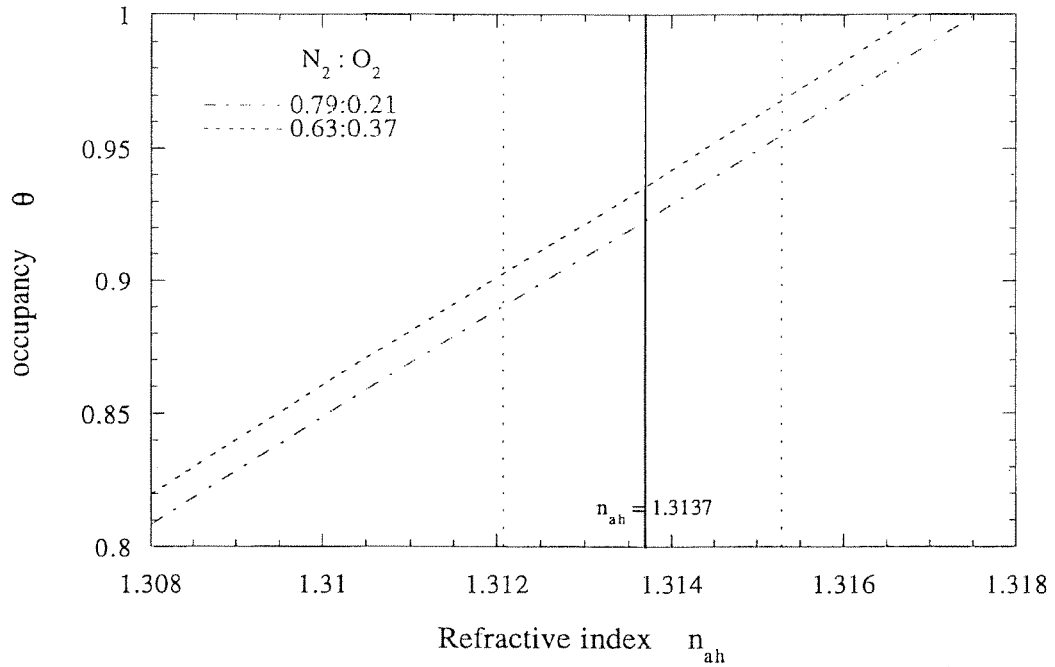

Figure 7: Relation between the cage occupancy and refractive index of air hydrate crystals. Two lines are calculated by the Onsager cavity model with the labeled air compositions. The measured refractive index (thick solid line: $n_{ah} = 1.3137$) is also shown together with the experimental errors as thin dotted lines. (From Uchida et al. [38].)

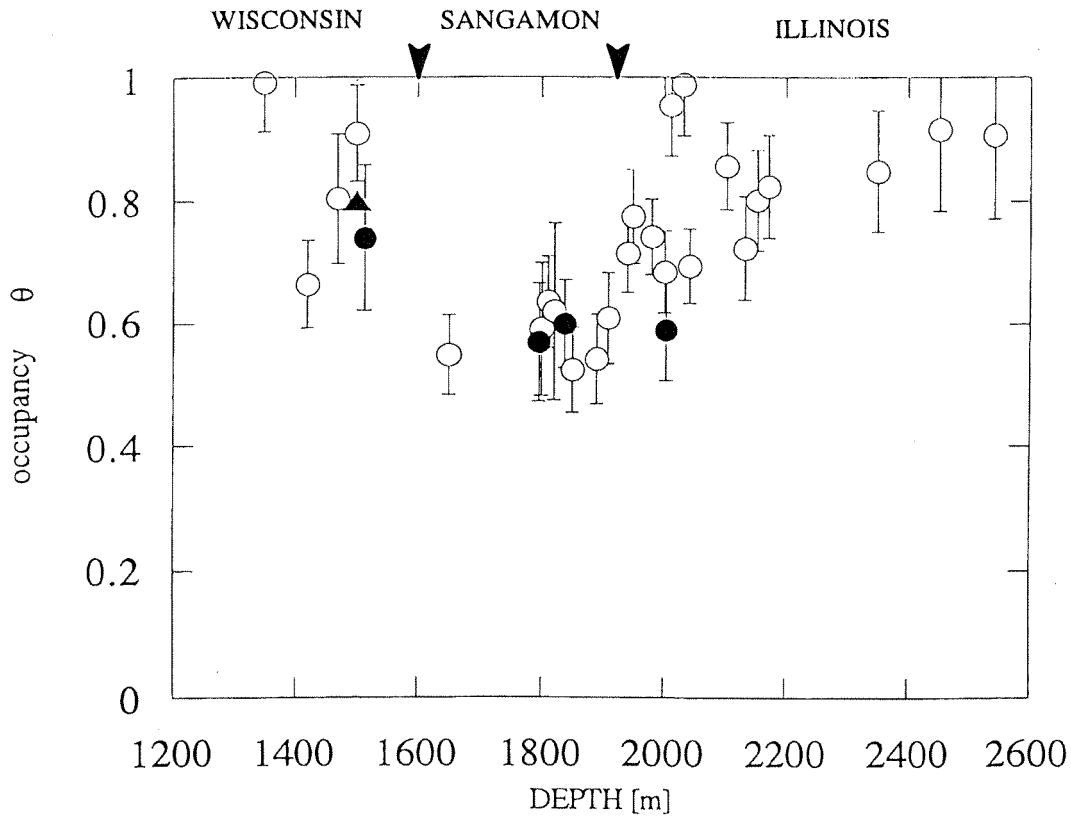

Figure 8: Variation of the cage occupancy θ with depth in Vostok ice cores as estimated from the volume concentration of air hydrates and the total gas content (modified for ref. 7). Two series of ice cores were used (solid and open circles). The solid triangle denotes the cage occupancy obtained by the refractive index measurements [38].

analyses. As described previously, ice core fracture does not occur after the transformation of air bubbles into air hydrates. Thus, to keep the ice core quality during storage and transportation, the mechanical properties of air hydrates and its interaction with surrounding ice matrix are important.

Air hydrate is one of the solid state inclusions which have different crystallographic structures with ice crystal, such as the volcanic microparticles, and is the primary inclusion in the deeper part of ice sheet. Thus, it is important to understand the mechanical interaction between air hydrates and the surrounding ice matrix. To evaluate this interaction, plastic and elastic mechanical properties of air hydrates should be summarized.

Measured mechanical properties of isolated air-hydrate crystals have not been reported because sufficiently large "pure" air-hydrate samples are difficult to obtain. However, the elastic phenomena are assumed to be similar to that of ice because the molecular configurations of the host lattice are essentially the same as in ice crystals: water molecules connect each other by the hydrogen bonding, and water molecules in both have four nearest

neighbors. The same Raman spectra between ice and air hydrates are found for the O-H stretching mode (approximately 3000–3800 cm^{-1}) and O-O bonding (200–350 cm^{-1}); this indicates that the elastic properties of air hydrates are close to those of ice [23]. However, Ikeda et al. [28] measured the Raman spectra of air hydrate crystals and showed that both modes related to H_2O molecules are shifted slightly from those of hexagonal ice crystals (see Table 1).

Kuhs et al. [19] measured the lattice constants and compressibility of the artificial N_2 hydrates by neutron diffraction, and found that the bulk modulus (the volume normalized pressure derivatives of the unit cell volume) for N_2 hydrate was

Table 1: Physical properties of air-hydrate crystals reported in the literature.

Property	Ice	Air hydrate
Space group [13]	$P6_3/mmc$	Fd3m
No. of H_2O molecules / unit cell [13]	4	136
Lattice parameter [$x10^{-10}$ m] [4, 13, 21]	a=4.52, c=7.36 (at 273K)	17.21, 17.23(average) (at 255 K), (at 273 K)
Linear thermal expansion [K^{-1}] [57, 21] (at 273 K)	$5.6x10^{-5}$	$4.4x10^{-5}$ (THF hydrate: $5.0x10^{-5}$) [estimated from 22]
Raman peak of guest molecules [23, 28]		
N-N str. in N_2 [cm^{-1}] (at 223 K)	-----	2323 (gas phase: 2328)
O-O str. in O_2 [cm^{-1}] (at 223 K)	-----	1547 (gas phase: 1554)
Raman peak of host molecules [28]		
O-H str. [cm^{-1}] (at 223 K)	3130	3135 (maximum peak)
O-O str. [cm^{-1}] (at 223 K)	219	211 (maximum peak)
N_2/O_2 ratio [23-28]		1.0～4.5 (atmosphere: 3.7)
Refractive index [38] (632.8 nm, 270.2 K)	1.3084(7)	1.3137(16)
Density [g cm^{-3}] [4, 38]	0.917	0.98～1.047 (depending on θ)
Cage occupancy by XRD [12, 13]		0.8 (θ_L: 0.6-1.0, θ_S: 0.7-0.8)
Cage occupancy by thermodynamic model [10]		0.86 (N_2 hydrate at 273 K)
Cage occupancy by Interferometer [38]		0.921～0.935(33)
Rheological coefficient [MPa yr] (at the threshold temperature where the activation energy change) [2]	～3	～30
Boundary energy [J m^{-2}] [58, 41]	Ice/Ice 0.065	Ice/Hydrate 0.063(12)
Partial molar volume [4, 17]		
water [m^3]	$2.88x10^{-29}$	$3.75x10^{-29}$
air [m^3]	------	$2.7x10^{-28}$

almost constant for pressures up to 0.25 GPa. It was slightly higher than the corresponding bulk modulus of ice I_h. The slight difference in the hydrogen bonding (compared to ice) observed by Raman spectra may be related to the difference of its bulk modulus to that of ice I_h.

On the other hand, the plastic mechanical properties of air hydrates can be estimated only from simulation using a physical model. A mathematical model [2] deduced the air-hydrate rheology by considering the diffusion coefficients of air and water molecules through an air-hydrate shell at an ice-air bubble interface. It predicted that hydrate crystals are at least one order harder than ice crystals.

Azuma and Higashi [40] discussed the effects of air-hydrates on the mechanical properties of ice cores. They did uniaxial compression tests on several deep ice cores from Dye-3 that contained air-hydrates to compare them with the mechanical properties of pure ice or ice cores with air bubbles. Air hydrates had no significant effect on the mechanical properties of ice cores.

Microscopic observations indicated air hydrate crystals pinned the grain boundary migration [41]. This is one indication of an interaction between air hydrates and the surrounding ice that is as effective as that from microparticles in ice. Therefore it is possible that air hydrates affect grain size variations in ice or the boundary migration of ice.

To estimate the effect of the hydrate existence quantitatively, Uchida et al. [41] measured the interfacial energy between air hydrate crystals and grain boundaries in ice by microscopic observations of air hydrates located on the ice grain boundaries. The interfacial energy γ_{ah} was close to that from the grain boundary γ_{gb} ($\gamma_{ah} = 0.97(\pm 0.19)\,\gamma_{gb}$). Then Uchida et al. [42] estimated the pinning effect of air-hydrates on the grain boundary migration. This value indicates that the pinning effect from an air hydrate crystal against the grain boundary migration is nearly that from volcanic microparticles. Shoji and Langway [6] also measured the value of γ_{ah}/γ_{gb} using a microscope to observe the melting of ice surrounding the hydrate. They reported that the ratio ranged from 4 to 7, depending on the hydrate crystal. Because of this large disagreement from different measurement techniques, additional precise measurements are needed to estimate the effect of air hydrates on the mechanical properties of the ice sheet.

As a summary of this section, we listed the physical properties of air-hydrate crystals in Table 1.

3. Air-hydrate formation in the ice matrix

Air hydrate crystals are transformed from air bubbles in ice sheets at certain depths. Fig. 9 shows a distinct region where air bubbles transform to air hydrates. From this figure, we can identify the following three depth regions where: (1) only air bubbles exist, (2) air hydrates coexist with air bubbles, and (3) only air hydrates exist. The formation of air hydrates includes two processes, nucleation and growth. The depth region of (2) is called "the transition zone", in which both nucleation and growth mechanisms might occur. But even after all air bubbles disappear (the depth region of (3)), air hydrate crystals can continue to grow [7]. We describe the transformation process from air bubbles to air hydrates in

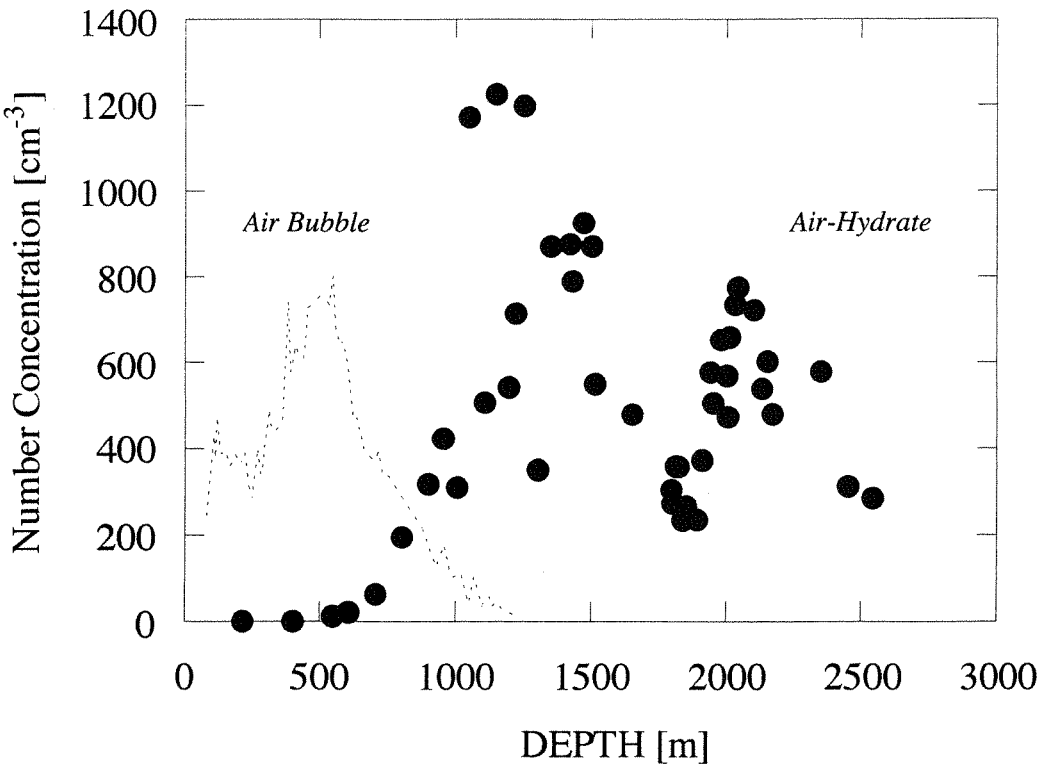

Figure 9: Depth variation of the number concentrations of both air bubbles (dotted line) and air hydrates (solid circles) in Vostok ice cores.

the transition zone in section 3.1 and the hydrate growth process at the depths with no air bubbles in section 3.2.

3.1 Air hydrate nucleation and the bubble-hydrate transition

The depth distribution of both air bubbles and air-hydrate crystals indicates that air-hydrate crystals gradually transform from air bubbles with depth. However, all air bubbles do not transform to air-hydrate crystals simultaneously: some air bubbles survive for several hundreds meter in depth or for several thousands year after the earliest nucleation events. In Vostok ice cores [7], for example, the transition zone is between about 500-m and 1250-m deep; this corresponds to a time period of 3–3.5×10^4 years [43]. The transition zone, therefore, is more than a hundred meters thick, which corresponds to a time period of more than a thousand years. To understand why air bubbles can survive in the transition zone even though the temperature and pressure conditions are under the hydrate stability conditions for this long, we should study the following: the (known) variations of gas compositions in both air bubbles and air hydrates with depth, and the driving force of the transformation and the nucleation-growth process of air hydrates.

The reason for the existence of the transition zone is thought to be due to the rate determining process of either hydrate nucleation or molecular diffusion (that is, that of the transformation process). Model

analyses and experimental studies have been done to evaluate each process.

The first model analysis to understand hydrate nucleation assumed homogeneous nucleation theory. Hondoh and Uchida [17] estimated the energy barrier of the hydrate nucleation on ice surface. They assumed that a rectangular nucleus ($L \times L \times h$) nucleated homogeneously on a smooth ice surface as shown in Fig. 10. The free energy change ΔG with the nucleation is then

$$\Delta G = -(L^2h/\Omega_g)\,\Delta\mu_g - (L^2h/\Omega_w)\,\Delta\mu_w + L^2\Delta\gamma + 4Lh\gamma_H \qquad (4)$$

where $\Delta\gamma$ is defined as γ_H (surface energy of hydrate) + γ_{IH} (interfacial energy between ice and hydrate) – γ_I (surface energy of ice), Ω_g and Ω_w are the molecular volumes in the hydrate of the guest and host, respectively.

Here we assume conditions of over-saturation $P>P_d$ (or supercooling $T<T_d$), where T_d is the dissociation temperature at pressure P_d. The chemical potential difference of guest molecules between the vapor and in the hydrate is

$$\Delta\mu_g = kT\,ln\,(P/P_d)\,. \qquad (5)$$

The chemical potential difference of water molecules between in ice and in the hydrate also can be written in terms of the supercooling $\Delta T = T_d - T$,

$$\Delta\mu_w = l_{IH}\,\Delta T/T_d\,, \qquad (6)$$

where l_{IH} is the latent heat of hydrate formation per water molecule. Since T_d can be related to P_d as in equation (2), i.e., $ln\,P_d = a - b/T_d$ (where a and b are constants), this equation is rewritten in terms of P_d.

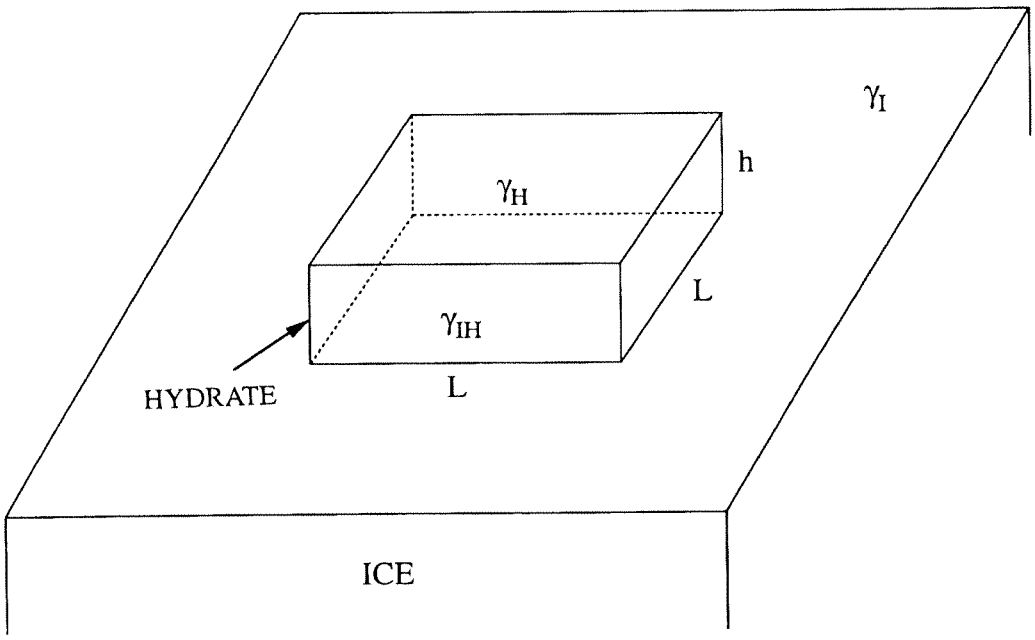

Figure 10: Illustration of the concept of hydrate nucleation on an ice surface [17]. The rectangular nucleus nucleated homogeneously on the smooth ice surface.

Then they estimated both the minimum radius of the nucleus, L_c, and the energy barrier of the nucleation, ΔG_c, as follows:

$$L_c = 4\,\gamma_H\,[(kT/\Omega_g + l_{IH}\,T/b\Omega_w)(ln\,P/\,P_d)]^{-1} \quad (7)$$

$$\Delta G_c = 16\,\gamma_H^2\,\gamma_{IH}\,[(kT/\Omega_g + l_{IH}\,T/b\Omega_w)\,ln(P/\,P_d)]^{-2}\,. \quad (8)$$

Here we assume $\gamma_H = \gamma_I$ and the nucleus shape has $h/L = \Delta\gamma\,/2\,\gamma_H$ to minimize ΔG. Assuming conditions in a deep ice sheet, the value of L_c from eq (7) was estimated to be at least $3.0\text{x}10^{-9}$ m and ΔG from eq (8) to be more than several hundred electron volts. This value is too large to explain the natural occurrence of air-hydrate crystals.

The experimental study of Ikeda et al. [44] indicated the nucleation rate of air hydrates in ice. They measured the transformation ratio of air bubbles to air hydrates under high hydrostatic pressures to infer the actual nucleation rate of air hydrates on air bubbles included in an ice matrix. They pressurized the ice samples, which included known numbers of air bubbles, for 16 days at 270 K and various hydrostatic pressures between 19.6 and 34.3 MPa. The number of air-hydrate crystals was measured after being pressurized. The comparison of these numbers indicated the transformation ratio of air-hydrate crystals at 270 K. They showed that the transformation ratio was approximately 0.5 % when $P/P_d = 2.4$. This result indicates that the hydrate nucleation was a heterogeneous process that lowered the high energy-barrier of the hydrate nucleation previously estimated by Hondoh and Uchida [17].

After air hydrates nucleate on an air bubble, the air bubble transforms to air-hydrate crystal. However, the microscopic observations of deep ice cores found no air hydrates during this transformation from the air bubble. This means that the transformation rate is fast compared to glaciological time scales.

To understand this transformation process, in situ observations of air-hydrate crystals from air bubbles were done under high hydrostatic pressures [45, 46]. The microscopic observations of air bubbles in the ice sample used a high-pressure vessel with optical windows and kept a constant temperature and pressure. Fig. 11 shows the transformation process observed under the microscope. The transformation starts at the interface between a bubble and ice. The hydrate growth is faster along the interface, but after it covers the interface, the hydrate grows toward the center of the bubble at a lower rate. The transformation was complete in less than one month under the experimental conditions. Each process was measured at various temperatures and pressures to deduce an activation energy of approximately 0.52 eV for the primary transformation along the interface and 0.90 eV for the subsequent growth inward. This result indicated that the rate determination process of the transformation to be mainly the supplement of water molecules to the transformation site.

At temperatures below 257 K, the transformation process was slightly different from that mentioned above [45]: the air bubble transformed gradually from one side to another after nucleation of the hydrate at the interface. This suggests that the relation between the supply rate of molecules and the formation rate varied with temperature.

Based on the above investigations, Price [5] proposed that the rate-determining process for the transformation from air

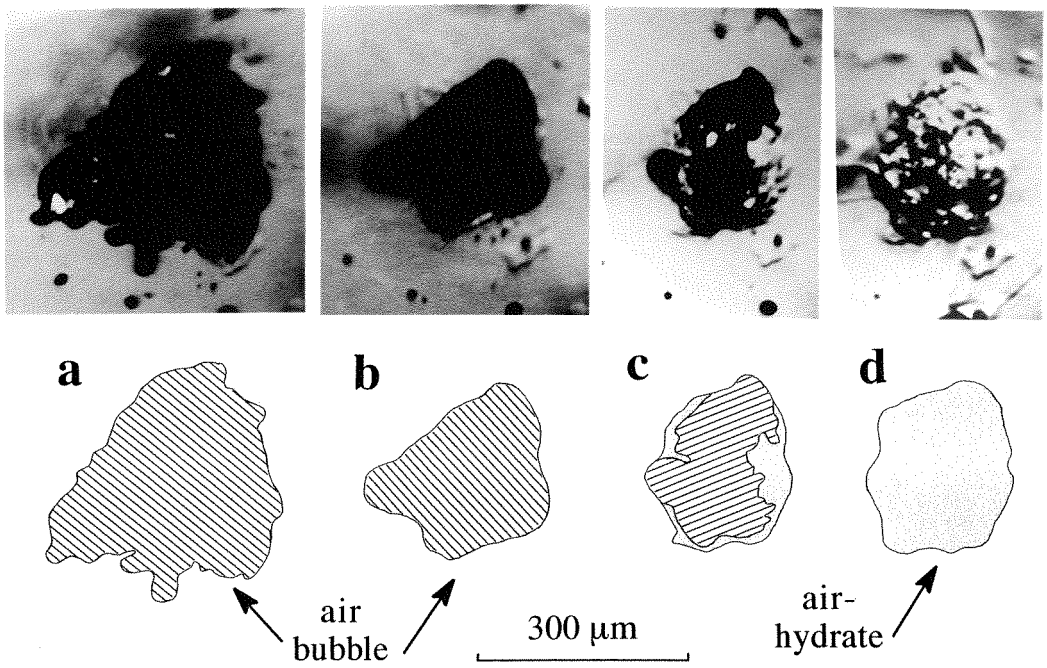

Figure 11: The transformation of an air bubble to hydrate crystal observed under the microscope with sketched outlines [46]. The total elapsed time is 164 hours.

bubbles to air hydrates to be the diffusion of water molecules through both ice and air-hydrate crystals. This is illustrated in Fig. 12a. Hondoh [47] pointed out, however, that Price's estimation of the diffusion coefficient of water in air-hydrate crystals was unreasonably low because it implied that the transition of all air bubbles would be incomplete until the end of the transition zone with the diffusion coefficient deduced by Price (see Fig. 12a-2). This suggestion is supported by microscopic observation of air-hydrate crystals in deep ice cores that found no partially-transformed air bubbles in the transition zone. This indicates that the rate-determining process is the nucleation of the hydrate (Fig. 12b).

To evaluate these processed quantitatively, a mathematical model of the post-nucleation stage of the bubble-hydrate conversion was developed by Salamatin et al. [2]. The model included the interaction between bubble compression and the diffusion of air and water molecules through the growing hydrate shell. Computation tests showed that the model parameters could be chosen to closely match the bubble-hydrate conversion rate observed in the laboratory experiments by Uchida et al. [46]. Using this theory, they concluded the following:

a. Due to low temperatures both in Greenland and Antarctica, the compressive deformation of the surrounding ice and the air-hydrate shells is the rate-limiting process in the post-nucleation transformation of air bubbles to hydrate crystals. Typical compression time scales range from 1 to

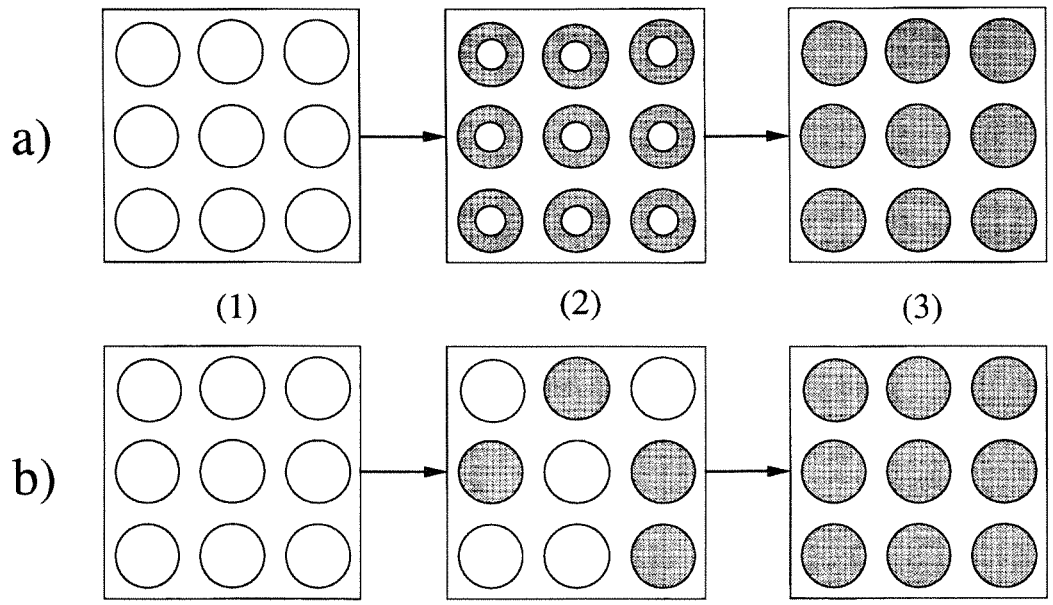

Figure 12: Illustration of the transformation process of air bubbles (open circles) to air hydrates (shaded part): a) the process controlled by water molecule diffusion [5], and b) the process controlled by hydrate nucleation [47].

100 years. Diffusion is too fast to influence the conversion time.

b. The bubble-hydrate transition zone in ice sheets covers a time interval three orders of magnitude longer than a typical time for post-nucleation crystal growth; therefore, air-hydrate formation is primarily controlled by the kinetics of hydrate nucleation.

These experimental and model simulation studies suggested that the long period of the transition zone mainly came from the difficulty of air-hydrate nucleation. Once air hydrates nucleated on an air bubble, the transformation period was approximately one-thousandth of the time period of the transition zone. This is why one does not find air-hydrate crystals partially-transformed from an air bubble (see Fig. 12a-2).

3.2 Growth of air hydrate in the ice matrix

The depth distribution of air-hydrates in deep ice sheet indicated that individual air-hydrate crystals grow even in the region without air bubbles. As described in section 2, air-hydrate crystals are constructed of both air and water molecules. The air-hydrate growth in deep ice sheets then requires a supply of air molecules and water molecule reconstruction from ice crystal to air-hydrate crystal. This process is much too slow to examine directly in the laboratory. However, understanding diffusion of air and water molecules in ice is very important to correctly interpret information from deep ice cores in which the annual layer becomes thinner with depth. In the present section, we review modeling

molecular diffusion related to hydrate growth.

Gas diffusion in the ice matrix is either through grain boundaries of ice crystals or through ice crystals. The former process is expected to be faster than the latter. However, a grain boundary is very thin compared to the size of a hydrate crystal. Hence, the total volume of gas diffusing through a grain boundary should be minor. Furthermore, because of the increase of ice grain size with depth, the effect of grain boundaries on air-hydrate growth should decrease with depth in an ice sheet. Fig. 13 shows the depth distribution of air-hydrates located on grain boundaries [42]. The probability of a hydrate existing on a grain boundary is approximately 0.6 at the bottom of the transition zone in Vostok ice and decreases with depth. Therefore, the main route of gas molecule diffusion in an ice matrix is assumed to be through the ice lattice.

The diffusion coefficients of air and water molecules were estimated by the model of air-hydrate transformation from an air bubble [2] that is described in the previous sections. The complete mathematical model indicates that the flux of water molecules from the ice to the air bubble is controlled by diffusion through the hydrate layer. The flux of air molecules in the hydrate layer is one or two orders of magnitude less than that of water molecules

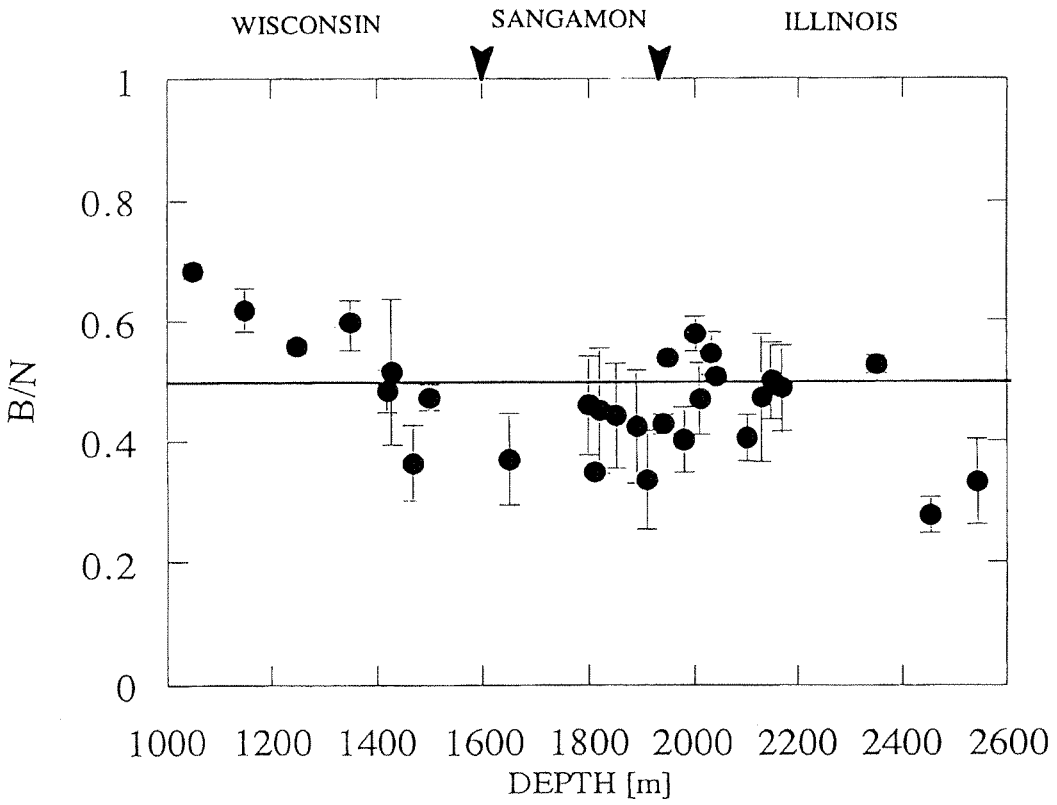

Figure 13: The probability (B/N) of a hydrate existing on a grain boundary in a Vostok ice core. (From Uchida et al.[42].)

in the opposite direction, but the latter cannot be neglected because it controls the bubble pressure and the diffusion rate at the final stage of the conversion. The effective mass transfer coefficient D of the diffusive transport of water and air molecules in air-hydrate crystal is estimated to be 0.6～1.3 $mm^2 \cdot yr^{-1}$ (1.9～4.1 x 10^{-10} $m^2 \cdot s^{-1}$) at 263 K. with a diffusion activation energy less than 30～50 $kJ \cdot mol^{-1}$ (0.31～0.52 eV). It is mainly determined by the self-diffusion coefficient of water (0.55～1.27 $mm^2 \cdot yr^{-1}$, i.e. 1.74 ～ 4.03 x 10^{-10} $m^2 \cdot s^{-1}$), which appears to be one order of magnitude larger than that in the ice lattice. Conversely, the diffusion coefficient of air in air-hydrate is small, D_{ha} = 0.05～0.4 $mm^2 \cdot yr^{-1}$ (0.16～1.3 x 10^{-10} $m^2 \cdot s^{-1}$), which is estimated to be at least two orders of magnitude less than the diffusion coefficients of the air constituents in ice.

Salamatin et al. [2] proposed a hydrate growth model that included the molecular diffusion process. Assuming a spherical bubble with a hydrate shell (see Fig. 14), the rate the hydrate volume V_h decreases or increases can be expressed as

$$dV_h/d\tau = 4\pi D\,(r_b\, r_h / (r_h - r_b))((P_b - P_d)/P_d) \quad (9)$$

where τ is time, r_b and r_h are the radii from the center of the sphere to the outer and inner boundaries of the hydrate shell, respectively. P_b and P_d are the pressures of the air bubble and hydrate dissociation, respectively. D is written

$$D = (1-y_d)\, D_{ha}/y_d + \nu C_d D_{hw}\,, \quad (10)$$

where D_{ha} and D_{hw} are the respective diffusion coefficients of air and water in hydrate crystals at equilibrium when P_b is close to P_d, ν is the number of cages per water molecule (3/17), and C_d is the concentration of water interstitials at hydrate equilibrium. The best fitting of the computation with the experimental data [46] indicated that D was between 1.4×10^{-14} and 2.6×10^{-14} $m^2 \cdot s^{-1}$ at 263 K. Assuming a process similar to the self-diffusion coefficient of water molecules in ice crystals, the diffusion coefficient of water molecules in the hydrate crystal was one order of magnitude greater than that in ice crystals at the same temperature. The diffusion coefficient of air in air hydrate crystals is estimated to be between 1.6×10^{-15} and 1.3×10^{-14} $m^2 \cdot s^{-1}$ when the total cage occupancy is 0.8.

Besides of the model estimation of the diffusion coefficient of air molecules in hydrate, we should know the diffusion of air molecules in the ice lattice to understand the transformation and growth processes of air hydrate crystals at depths without air bubbles. One estimate of the gas molecule diffusion through the ice lattice using the observations of hydrate distributions was proposed by Uchida et al. [48]. Diffusion of gas molecules through ice between two hydrate crystals with different diameters causes the larger crystal to grow and the smaller crystal to shrink. From their data on Vostok cores deeper than 1050 m, they found the following:

(1) the average radius of the hydrate crystals increased with depth at a rate of 0.16 $\mu m \cdot kyr^{-1}$ (5.07 x 10^{-18} $m \cdot s^{-1}$)
(2) this increment was due to shrinkage of the hydrate crystals with radii less than 67 μm
(3) the number densities of hydrate crystals with radius r varied with time depending on r.

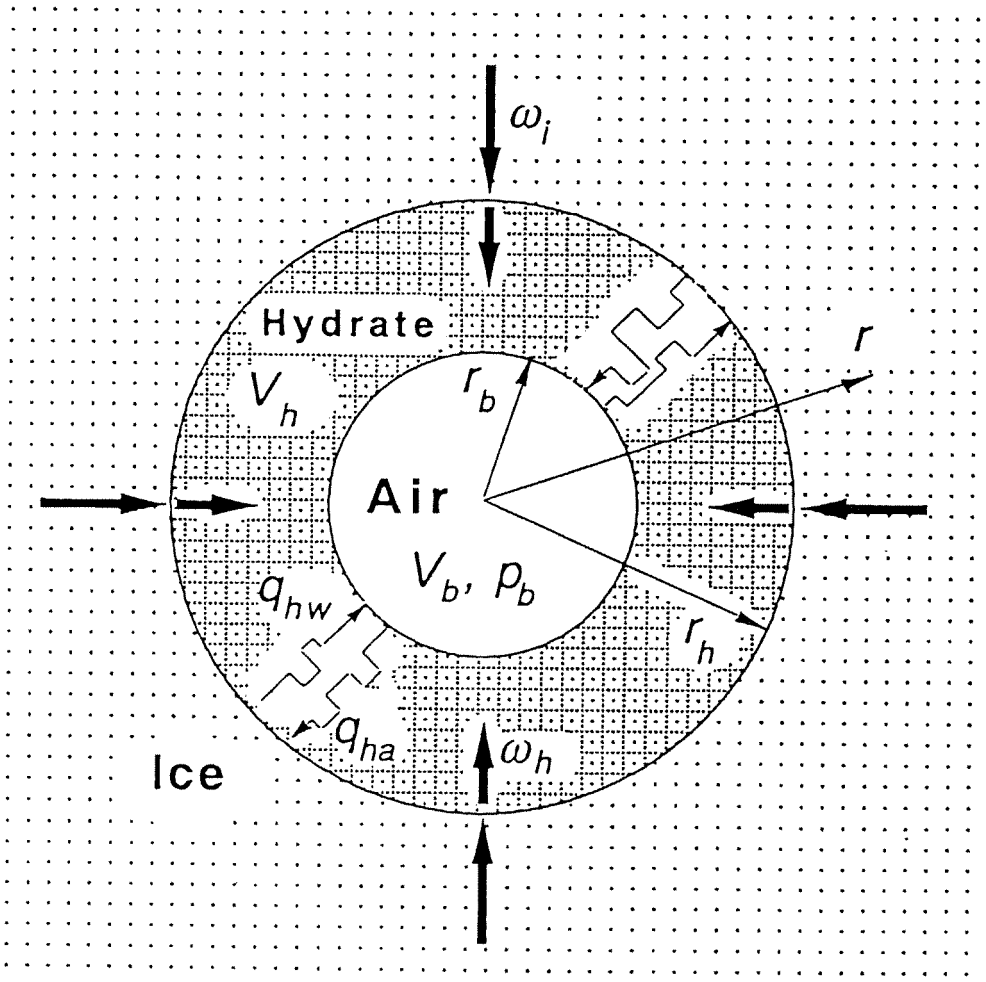

Figure 14: A hydrate growth model that includes molecular diffusion and assumes a spherical bubble with a hydrate shell. Here r_b is the bubble radius, r_h is the external radius of the air hydrate shell. ω_h and ω_I denotes the volume deformation rate of the hydrate shell and of the surrounding ice, respectively. q_{ha} and q_{hw} are the mass fluxes through the spherical hydrate shell of air and water, respectively. (From Salamatin et al. [2].)

Then they used a two-body approximation for the diffusion analysis to calculate the value of $D_g C_{ge}$, where C_{ge} is the equilibrium concentration of air molecules in ice. As a result, $D_g C_{ge}$ is of order 10^{-19} $m^2 \cdot s^{-1}$ for conditions deep in ice sheets.

Diffusion coefficients of the gases, however, are too small to be accurately measured directly. Satoh et al. [49] measured the diffusion coefficients of noble gases He, Ne and Ar in ice crystals instead of N_2 and O_2. They obtained the following linear relationship between the diffusion coefficients D_g $m^2 \cdot s^{-1}$ and the van der Waals radius of the noble gas molecules R_{vw} (m):

$$D_g = 4.0\text{x}10^{-4} \exp(-R_{vw} / R_c) \qquad (11)$$

at 263.2 K where R_c equals $1.05\text{x}10^{-11}$ m. The temperature dependence of D_g was not determined due to the small temperature range they used (between 258.2 K and 268.2 K). Extrapolation of this relation to the radii of $2.05\text{x}10^{-10}$ m, $2.10\text{x}10^{-10}$ m, and $2.56\text{x}10^{-10}$ m allows the diffusion coefficients of N_2, O_2, and CO_2 to be estimated at $1.4\text{x}10^{-12}$ $m^2 \cdot s^{-1}$, $8.7\text{x}10^{-13}$ $m^2 \cdot s^{-1}$, and $1.0\text{x}10^{-14}$ $m^2 \cdot s^{-1}$, respectively. Because D_g strongly depends on R_{vw}, small differences in the radius gives a large difference in D_g; thus, the results given above depends on the values assumed for the radii.

These values, ranging from 0.87 to 1.4 $\text{x}10^{-12}$ $m^2 \cdot s^{-1}$ for O_2 and N_2 molecules in ice lattice, are two orders of magnitude larger than the diffusion coefficient of air molecules in the hydrate estimated by Salamatin et al. [2] ($0.16 \sim 1.5\ \text{x}10^{-14}$ $m^2 \cdot s^{-1}$). This suggests that air molecules are difficult to diffuse in the hydrate lattice compared to the ice lattice due to a higher energy barrier for molecular jumps between neighboring cages.

Satoh et al. [49] also determined the equilibrium concentrations of Helium and Neon in ice single crystals. The molar fractions are $2.5\text{x}10^{-6}$ for Helium and $3.5\text{x}10^{-7}$ for Neon. These values are averages over the temperature range between 258.2 and 268.2 K. Since these values were estimated with a pressure of 0.1 MPa, the molar fraction at a pressure P MPa should be multiplied by $10P$. In addition, assuming a similar dependence on R_{vw} as equation (11), the estimated equilibrium concentration for N_2, O_2 and CO_2 are $1.4\text{x}10^{-8}$, $1.1\text{x}10^{-8}$ and $7.7\text{x}10^{-10}$, respectively.

Later, the estimation of the van der Waals radii of both N_2 and O_2 molecules was found to be wrong. The correct estimation of the diffusion coefficients and of the gas concentrations by using the same equations, but with the new radii are as follows:

$$C_{N2} = 1.8\text{x}10^{-8},\ C_{O2} = 2.6\text{x}10^{-8}\ \text{MPa}^{-1} \quad \text{at 263 K, 0.1MPa} \qquad (12\text{-}1)$$

$$D_{N2} = 1.4\text{x}10^{-12},\ D_{O2} = 2.2\text{x}10^{-12}\ m^2 \cdot s^{-1} \quad \text{at 263 K, 0.1MPa} \qquad (12\text{-}2)$$

Using these values, the product $D_g C_{eg}$ becomes 10^{-18} $m^2 \cdot s^{-1}$ at 263 K and 10MPa. This value is one order of magnitude more than that estimated from the distribution observations.

For the estimation of the diffusion coefficients of N_2 and O_2 molecules in ice, Ikeda et al. [11, 27] proposed a different estimation method from that which is above; it is based on their assumption of the D_g dependence of the molecular jumping rate between interstitial sites in an ice lattice. The details of the calculation are in Ikeda et al. [11]. As a result, the estimated diffusion coefficient of N_2 is approximately $2\text{x}10^{-13}$ $m^2 \cdot s^{-1}$ and that of O_2 is $5\text{x}10^{-13}$ $m^2 \cdot s^{-1}$, both at 263 K. These values multiplied by the values in (12-1) are close to the estimate of $D_g C_{ge}$ obtained from the hydrate distributions. Furthermore, the result obtained by Ikeda et al. [11, 27] indicated that $D_{N2} < D_{O2}$, which was the opposite conclusion to that in Sato et al. [49].

Recently Salamatin et al. [43] summarized data in the literature on gas diffusion in the ice lattice. They concluded that the diffusive permeation coefficient of N_2 and O_2 molecules in ice are

$$D_{N2}C_{N2} = 3.4 \times 10^{-19}\ m^2 \cdot s^{-1} \quad (13\text{-}1)$$

$$D_{O2}C_{O2} = 1.3 \times 10^{-18}\ m^2 \cdot s^{-1} \quad (13\text{-}2)$$

These results verify that the diffusive permeation coefficient of O_2 is noticeably greater than that of N_2. Furthermore, if the difference in temperature is taken into account, they agree with that of air molecules ($10^{-20} \sim 10^{-19}\ m^2 \cdot s^{-1}$ at 233 K and 10 MPa) estimated from the hydrate distribution.

The relation of $D_{N2} < D_{O2}$ also suggests that the difference of the diffusion rate of both gas molecules through ice lattice and the hydrate shell could cause a change of the N_2/O_2 ratio during bubble-hydrate transformation (i.e., fractionation). Ikeda et al. [11, 27] measured the depth distribution of N_2/O_2 ratio both in air bubbles and in air-hydrate crystals in Vostok ice cores by Raman spectroscopy. The N_2/O_2 ratio in the air bubble is the atmospheric value at the beginning of the transition zone, but increases with depth down to the bottom of the transition zone. An excess of O_2 in the hydrates should balance the excess of N_2 in the air bubbles. The N_2/O_2 ratios in the hydrates were smaller than those in the present air at the beginning of the transition zone, and asymptotically approached the atmospheric value as the transition progressed. They concluded that this very large fractionation was attributed to faster diffusion of O_2 molecules from air bubbles to air hydrates through the ice lattice as compared to N_2.

The above mechanisms are supported qualitatively by the depth distribution of the hydrate morphology. Fig. 15 shows the variations of the stratigraphies of air hydrate crystals in Vostok ice cores. At the depths of the transition from air bubbles to air hydrates, the shape of the hydrate retains the shape of the air bubble based on a microscopic observation study [7]. So the major stratigraphy of air hydrates is spherical at the shallower part of the transition zone. Conversely, faceted crystals dominate in the deeper parts of the transition zone. This is probably because the air hydrate crystals are growing, using nearby air bubbles as a source of air molecules. In this region, oxygen molecules are assumed to diffuse preferably. After all air bubbles disappear, the source of the air molecules for the hydrate growth must be other air hydrates. At that depth, the sharp edges of the crystal round off and spherical hydrates again dominate. The same tendency in the stratigraphic distributions was reported in GRIP deep ice cores [50].

Fig. 15 also shows another morphology: irregular type. An X-ray diffraction study indicated that irregular type crystals were usually polycrystals (Anzai, personal communication). The formation process of this type might be different from that explained above. Another mechanism to form a hydrate crystal that might explain polycrystals is coalescence of the hydrate crystals, which is not well understood yet. Fig. 16a shows an irregular-type air hydrate typical of those observed in the transition zone of Vostok ice. This crystal looks like a group of crystals, each smaller than 10 μm in close proximity. Below the transition zone, irregular-type crystals have a slightly different shape as shown in Fig. 16b: the crystal becomes one isolated body instead of a group of small crystals. One of the possible interpretations of this change is the coalescence of the small crystals. As discussed above, the smaller hydrate has a larger driving force for molecular diffusion

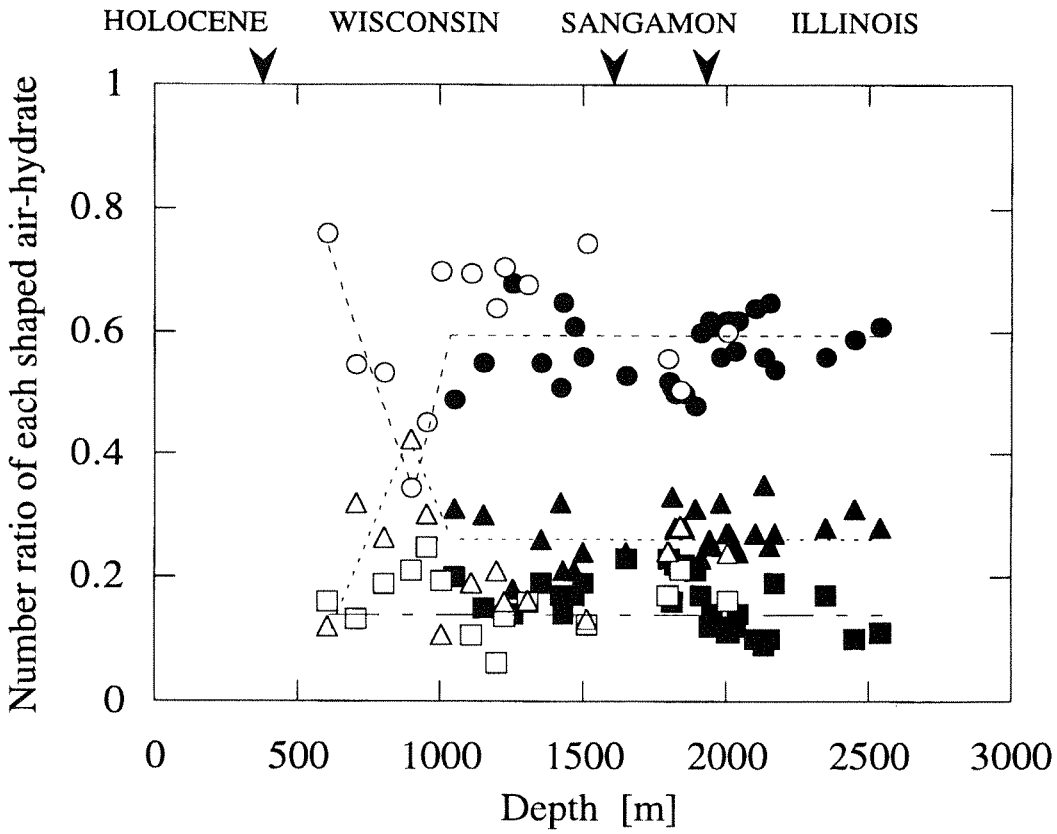

Figure 15: Variations of the stratigraphies of air hydrate crystals in Vostok ice cores. Spherical crystal: Ns/N (circle), irregular: Ni/N (square), and faceted: Nf/N (triangle) for two series of ice cores (open and solid marks). (From Uchida et al. [7].)

[48]. Therefore the small crystals might easily coalesce with each other after all the air bubbles disappear.

The formation process of the irregular type hydrate has not been determined, although Salamatin et al. [2, 43] suggested that it was from the breaking of the hydrate shell followed by further recrystallization of the pieces. Their model simulation suggested that these broken air-hydrate shells form mainly in the middle of the transition zone.

Lipenkov [51] found significant changes in the distribution of hydrate crystals in his optical microscope observations of the Vostok cores. The hydrate crystals were uniformly distributed over the core samples in shallower regions, as was the distribution of air bubbles. However, a non-uniform distribution gradually developed as the depth increased. This change in the distribution seems to be caused by migration of small crystals toward larger ones. Migration of the hydrate crystals may occur due to a non-uniform distribution of gas molecules around the small hydrate crystals, or due to migration of grain boundaries in ice, which carry the small hydrate crystals.

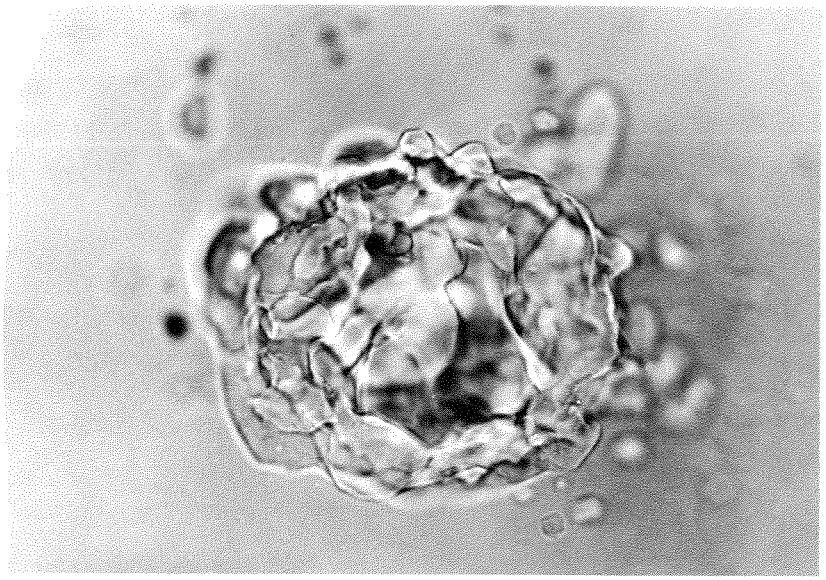

(a) 100 μm

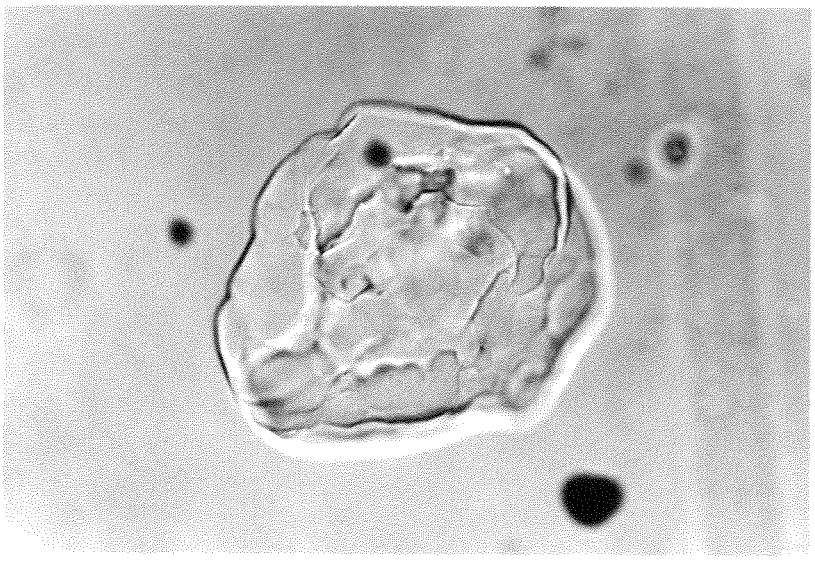

(b) 100 μm

Figure 16: Typical shapes of irregular-type air hydrates in Vostok ice cores: a) in the transition zone (1050-m deep), and b) below the transition zone (1800 m).

4. The stability conditions and the dissociation process of air-hydrates

Shoji and Langway [6] observed air-hydrates in several deep ice cores. The shallowest depths at which air hydrates were observed in the Dye-3, Camp Century (Greenland), and Byrd Station (Antarctica) cores were at 1092-m, 1099-m, and 727-m depths, respectively. They concluded that, for the Dye-3 and Camp Century cores, the observed depths that air-hydrate first appear agreed with equation (1). (See Fig. 17.) According to this result, Miller's phase diagram of air hydrate [1] is useful for estimating the approximate distributions of air hydrates and air bubbles. In section 4.1, we compare Miller's phase diagram with the actual distribution of both air bubbles and air hydrates. Then we discuss the reason for the long-period survival of hydrates in ice cores that were stored under unstable conditions for air hydrates. This abnormal stability of air hydrates in ice cores is also discussed in relation to observations of air-hydrate dissociation in an ice matrix. In section 4.2 we show that the dissociation process suggests an optimal condition for ice core storage.

4.1 Air hydrate distributions and the collection of Miller's diagram

As described in the section 1, the dissociation pressure of air hydrates P_d can be predicted using the following equation:

$$P_d = X_{N2}{}^H P_{N2} + X_{O2}{}^H P_{O2}, \quad (14)$$

where $X_{N2}{}^H$ and $X_{O2}{}^H$ are the mole fractions in the hydrate phase. Equation (14) can be represented in terms of the mole fractions in the gas phase as follows [2]:

$$P_d = (P_{N2} \cdot P_{O2}) / (X_{N2} P_{O2} + X_{O2} P_{N2}). \quad (15)$$

(In the original paper [2], the term of P_{O2} was missing.) Then the mole fraction of component i in the hydrate phase, X_i^H, can be related to that in the gas phase at equilibrium, i.e.,

$$X_i^H = P_d X_i / P_i. \quad (16)$$

Fig. 17 shows the variations of dissociation pressures with the mole fraction of nitrogen at $T = 270.5$ K. If $X_{N2}{}^H$ is approximately 0.8, then X_{N2} is 5 % larger than $X_{N2}{}^H$. The difference in the estimated dissociation pressure using $X_{N2}{}^H$ compared to that using X_{N2} is approximately 0.2 MPa. This distinction should be included when one transports and stores ice cores to avoid dissociation of air hydrates.

Fig. 18 shows that the shallowest observation of air hydrates are at a slightly higher pressure than that estimated from equation (15). This slight disagreement is attributed to the difficulty of hydrate nucleation. For the Byrd Station cores, on the other hand, the observed depth that hydrates first appeared was approximately 100-m shallower than that predicted by Miller's diagram. Craig et al. [52] analyzed this discrepancy and suggested that it was due to the generally upward ice flow trajectory at Byrd Station, which began approximately 5-km upstream from the Byrd Station location. They proposed that air hydrates were the indicator of "a paleopiezometer" for the polar ice cap.

It is well known that high-quality hydrate crystals have been kept in ice cores for more than ten years even though the dissociation pressure of air hydrates is much higher than atmospheric at the storage temperature. This had been explained as

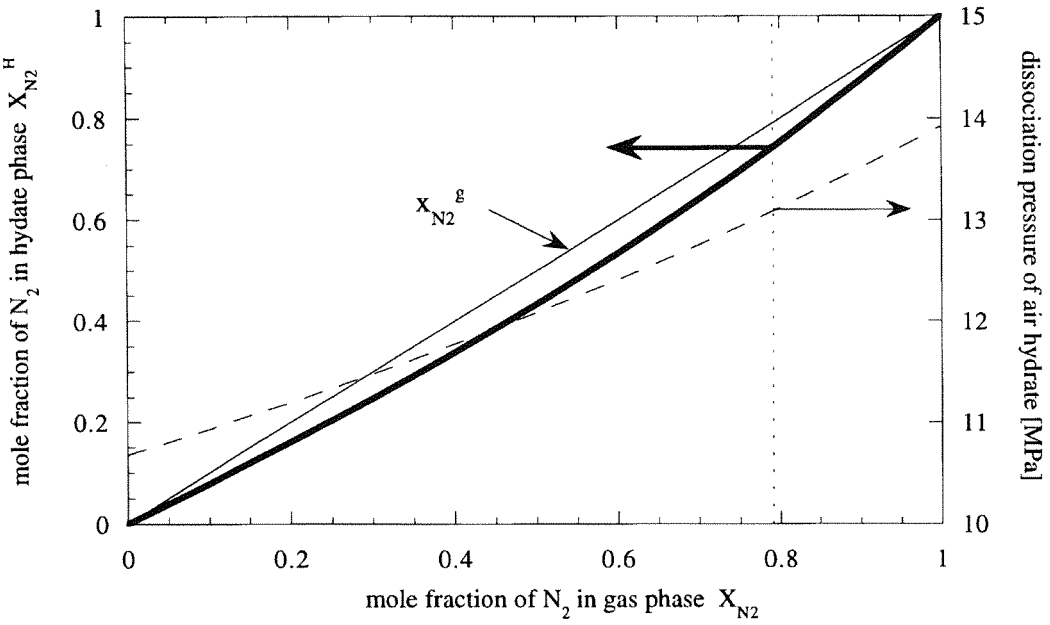

Figure 17: Variations of dissociation pressures with the mole fraction of N_2 at T = 270.5 K. The solid line and the dotted line indicate the dissociation pressures at the mole fraction of N_2 in the hydrate phase and in the gas phase, respectively.

being caused by the ice matrix functioning as a pressure vessel for air-hydrate crystals to prevent their dissociation. However, this explanation might be incorrect because the ice matrix easily deforms under such high pressure. Now, it is assumed that bubble nucleation on the hydrate crystal is the key to understanding the abnormal stability of air hydrates in ice. High-pressure bubbles formed by air-hydrate dissociation could cause ice core fracture. Therefore, the ice core quality can be kept high if no air hydrates dissociate.

Since air hydrate crystals are solid particles, they are expected to affect the mechanical properties of the surrounding ice matrix. For example, serious damages on ice cores were observed when they were recovered from severed hundred meters in depth (the hatched area in Fig. 18). This depth range is known as the brittle zone. The high-pressure bubbles are assumed to fracture the ice. This ice fracture ceased with the transformation of air bubbles to air-hydrate crystals. Uchida et al. [53] discussed this process quantitatively.

Some researchers reported a similarly abnormal stability of gas hydrates coexisting with ice crystals [4, 54]. This is known as the "self-preservation effect". In permafrost areas, natural gas hydrates were observed at abnormally shallow depths, owing partly to this effect. This hydrate is thought to be a dominant source of greenhouse-effect gases because it would easily dissociate if an atmospheric temperature rise propagates into the shallower regions of the permafrost. Therefore, the self-preservation effect is now an important problem in hydrate research.

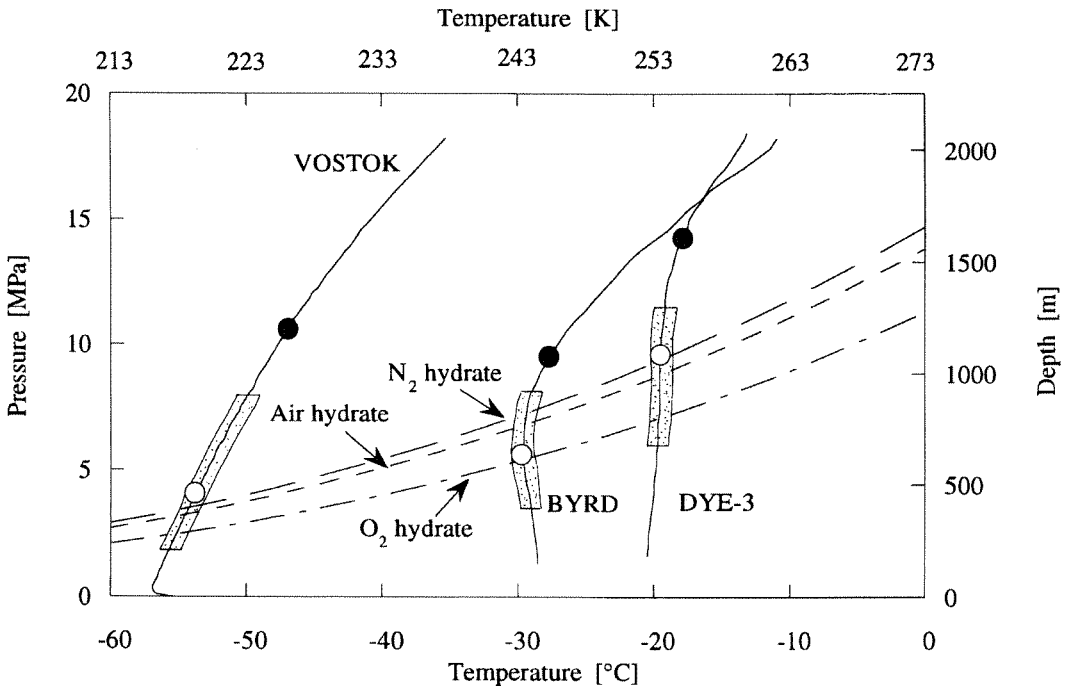

Figure 18: Composite diagram of the air-hydrate experiment on deep ice core samples (modified for ref 2, 6 and 55). ○: first air hydrate occurrence, ▨: brittle zone, ●: air bubble disappearance in ice cores, and dissociation curves are calculated from equations (15), (2-1), and (2-2) for air hydrate, N_2 hydrate, and O_2 hydrate, respectively. The depth distributions of air hydrates were from Dye-3, Camp Century (Greenland), and Byrd Station (Antarctica) [6].

4.1 Dissociation process of air hydrates and optimized conditions for the sample storage

To control the dissociation of air hydrates in ice cores, we should study the dissociation process of air hydrates. The bubble nucleation conditions at the interface between air hydrate and surrounding ice can be estimated quantitatively using its interfacial energy [41]. If we use the analogy of hydrate nucleation on the air bubble to the bubble nucleation at the interface between the air hydrate and ice (section 3.1), the critical radius of the bubble nucleus and the free energy of the formation of the critical nucleus are similar to those estimated in the homogeneous nucleation of the hydrate on the bubble surface. Therefore, air bubble nucleation at the interface between air hydrate and ice is very difficult without any help from nucleation-induced processes.

Using a microscope, Shoji and Langway [4, 55] observed nucleation of air bubbles on air hydrate crystals. They found that the transformation process from air hydrates to bubbles was clearly related to strain-induced nucleation. In particular, air bubbles easily nucleated when the inclined slip plane of the surrounding ice crystal contacted the hydrate surface.

Another possibility that could explain the observed bubble nucleation is the temperature difference that is induced by

the difference of the linear thermal expansions between ice and hydrates. As mentioned in section 2.1, the thermal expansion of an air hydrate crystal is slightly smaller than the surrounding ice crystal [21]. If the storage temperature increases, the air hydrate crystals will have tensile stress. This could be the driving force for bubble nucleation on the hydrate crystal. Experimental and model simulation studies should be done to evaluate this mechanism of bubble nucleation.

After nucleation of air bubbles at the interface between ice and air hydrate, the hydrate dissociates relatively quickly. Microscopic observations [6, 7] of the dissociation process found the following sequence of events: First, an air bubble nucleated at the interface. The air bubble then grew along the hydrate crystal. The pressure of the bubble was as high as that for hydrate equilibrium at that temperature. This expanded the bubble into cracks induced by the elastic deformation of ice [53] (i.e., the formation of micro-cracks, or the fracture of ice matrix) or by the plastic deformation of ice.

Uchida et al. [56] also observed air-hydrate crystals in ice cores stored at different conditions. They found a storage-temperature dependence on the air-hydrate dissociation in ice cores. If the storage temperature was high enough to accelerate the relaxation of ice cores by its plastic deformation, the hydrates would dissociate to make high-pressure bubbles that resulted

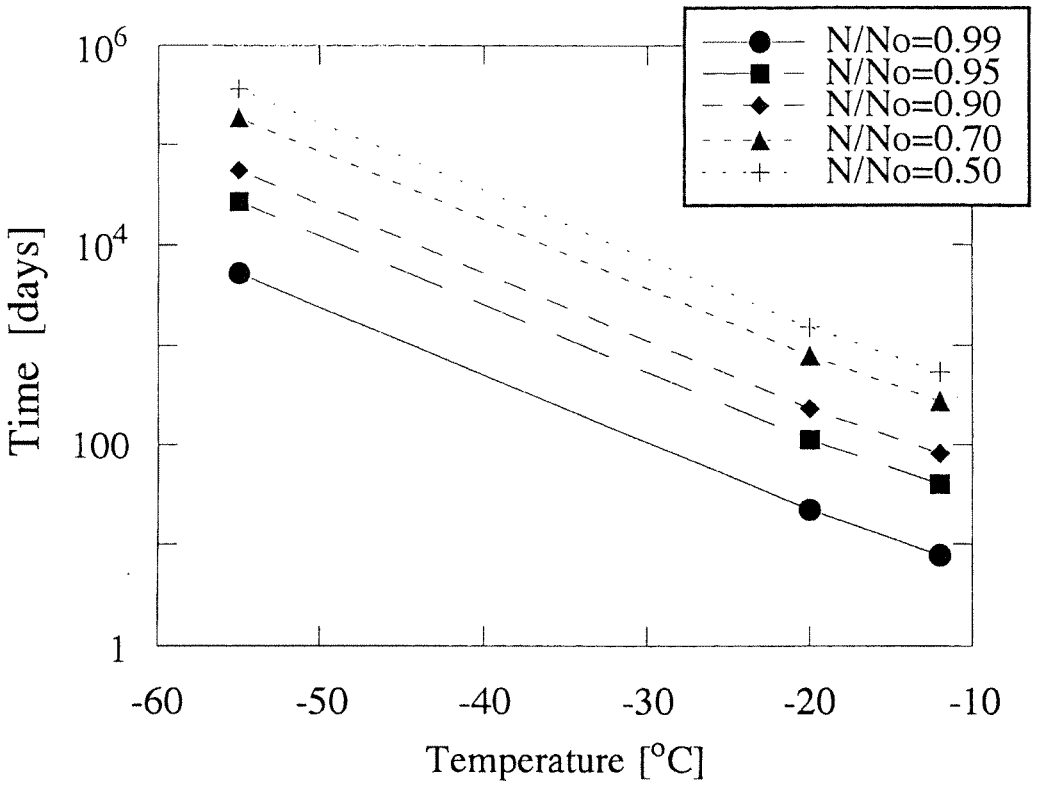

Figure 19: Calculation of the fraction (N/N_0) of hydrates remaining in an ice core as a function of the storage temperature and time period. (From Uchida et al. [56].)

in ice-core fracture. These findings suggest that the air-hydrate to bubble transformation process is strongly controlled by the nucleation activation process during and after ice core recovery. Therefore, temperature control is important for the safe storage of ice cores and for their successive analyses.

These analyses [56] suggest optimal transportation and storage conditions of deep ice cores to maintain a high quality of samples. Fig. 19 illustrates the storage temperature and time period dependence of the dissociation ratio from 1 to 50 %. For example, if the ice core is stored at –20 ℃ (253.2 K) for 90 days, approximately 4 % of the air-hydrate crystals will dissociate. For the long term storage of ice cores, i.e., 10 years or more, the temperature should be below –53 ℃ (220.2 K) to keep the dissociation ratio of air-hydrate crystals less than 1 %. Using this diagram, the temperature condition of transportation and storage for ice cores were planned at the deep ice core-drilling project in the Japanese Antarctic Research Expedition. Also, the temperature of the cold room in the Institute of Low Temperature Science, Hokkaido University, is controlled at approximately 220 K.

Acknowledgments

We acknowledge all members of both the Faculty of Engineering (supervised by Professor S. Mae) and the Institute of Low Temperature Science (supervised by T. Hondoh) in Hokkaido University who contributed to the air hydrate analysis. We also thank to Dr. V. Ya. Lipenkov, Dr. P. Duval, Professor A. N. Salamatin, Dr. F. Pauer, Dr. W. F. Kuhs, Professor H. Shoji, Dr. A. Higashi, Professor H. Craig, the late Professor T. Kuroda for their fruitful discussions.

References

1. S.L. Miller, *Science*, 165, 489 (1969)
2. A.N. Salamatin, T. Hondoh, T. Uchida, V.Ya. Lipenkov, *J. Cryst. Growth*, 193, 197 (1998)
3. H. Shoji and C.C. Langway, Jr., *Nature*, 298, 548 (1982)
4. E.D. Sloan, Jr., *Clathrate Hydrates of Natural Gases*, 2nd ed., revised and expanded, Marcel Dekker, Inc., New York, pp. 26 (1998)
5. P.B. Price, *Science*, 267, 1802 (1995)
6. H. Shoji and C.C. Langway, Jr., *J. Physique*, 3, C1-551 (1987)
7. T. Uchida, T. Hondoh, S. Mae, V.Ya. Lipenkov, and P. Duval, *J. Glaciol.*, 40, 79 (1994)
8. V.Ya. Lipenkov, (in this volume)
9. M. Fujii, *Master Thesis*, Hokkaido University (1997)
10. W.F. Kuhs, A. Klapproth and B. Chazallon (in this volume)
11. T. Ikeda, A.N. Salamatin, V.Ya. Lipenkov and T. Hondoh (in this volume)
12. H. Anzai, *Master thesis,* Hokkaido University (1988)
13. T. Hondoh, H. Anzai, A. Goto, S. Mae, A. Higashi, and C.C. Langway, Jr., *J. Inclus. Phenom. Molec. Recogn. Chem.*, 8, 17 (1990)
14. D.W. Davidson, in *Water – A Comprehensive Treatise*, (ed. by F. Franks), Plenum Press, New York, Vol. 2, Chap. 3, pp. 115 (1972)

15. D.W. Davidson, Y.P. Handa, C.I. Ratcliffe, J.S. Tse, and B.M. Powell, *Nature*, 311, 142 (1984)
16. D.W. Davidson, S.R. Gough, Y.P. Handa, C.I. Ratcliffe, J.A. Ripmeester, and J.S. Tse, *J. Physique*, 48, CI-537 (1987)
17. T. Hondoh, and T. Uchida, *Low Temp. Sci., Ser. A*, 51, 197 (1992) (in Japanese)
18. J.H. van der Waals, and J.C. Platteeuw, *Adv. Chem. Phys.*, 2, 1 (1959)
19. W.F. Kuhs, B. Chazallon, A. Klapproth, and F. Pauer, *J. Inclus. Phenom.*, 29, 65 (1997)
20. W.F. Kuhs, B. Chazallon, A. Klapproth, and F. Pauer, *Rev. High Pressure Sci. Technol.*, 7, 1147 (1998)
21. S. Takeya, H.Nagaya, T. Hondoh, T. Matsuyama, V.Ya. Lipenkov, *J. Phys. Chem. B* (in press)
22. J.S. Tse, *J. Physique*, 3, C1-543 (1987)
23. J. Nakahara, Y. Shigesato, A. Higashi, T. Hondoh, and C.C. Langway, Jr., *Phil. Mag. B*, 57, 421 (1988)
24. T. Ikeda, H. Fukazawa, S. Mae, L. Pepin, P. Duval, B. Champagnon, V.Ya. Lipenkov and T. Hondoh, *Geophys. Res. Lett.*, 26, 91 (1999)
25. H. Fukazawa, T. Ikeda, T. Hondoh, P. Duval, V.Ya. Lipenkov, and S. Mae, *Proc. of 2nd Int. Conf. on Natural Gas Hydrates*, 237 (1996)
26. F. Pauer, J. Kipfstuhl, and W.F. Kuhs, *Geophys. Res. Lett.*, 22, 969 (1995)
27. F. Pauer, J. Kipfstuhl, and W.F. Kuhs, *Geophys. Res. Lett.*, 23, 177 (1996)
28. T. Ikeda, H. Fukazawa, S. Mae, T. Hondoh, and C.C. Langway, Jr., *J. Phys. Chem. B*, 101, 6180 (1997)
29. P.M. Roger, *J. Phys. Chem.*, 94, 6080 (1990)
30. H. Tanaka and K. Kiyohara, *J. Chem. Phys.*, 98, 4098 (1993)
31. H. Tanaka and K. Kiyohara, *J. Chem. Phys.*, 98, 8110 (1993)
32. H. Tanaka, *J. Chem. Phys.*, 101, 10833 (1994)
33. J. Tabata, K. Kawamura, A. Goto, T. Hondoh and S. Mae, *Proc. Int. Conf. on Computer Applications to Materials and Molecular Science and Engineering*, 329 (1993)
34. N. Kumagai, K. Kawamura and T. Yokokawa, *Mol. Sim.*, 12, 177 (1994)
35. S. Horikawa, H. Itoh, J. Tabata, K. Kawamura, and T. Hondoh, *J. Phys. Chem. B*, 101, 6290 (1997)
36. P. Martinerie, D. Raynaud, D.M. Etheridge, J.-M. Barnola and D. Mazaudier, *Earth and Planetary Sci. Lett.*, 112, 1 (1992)
37. W.R. Parrish and J.M. Prausnitz, *Ind. Eng. Chem. Process Des. Devel.*, 11, 26 (1972)
38. T. Uchida, W. Shimada, T. Hondoh, S. Mae, and N. I. Barkov, *App. Opt.*, 34, 5746 (1995)
39. D.W. Davidson, R.N. O'Brien, P. Saville, and S. Visaisouk, *J. Opt. Soc. Am. B*, 3, 864 (1986)
40. N. Azuma, and A. Higashi, *Ann. Glaciol.*, 5, 1 (1984)
41. T. Uchida, S. Mae, T. Hondoh, P. Duval, and V.Ya. Lipenkov, *Proc. of the NIPR Symp. on Polar Meteorology and Glaciology*, 7, 1 (1993)
42. T. Uchida, S. Mae, T. Hondoh, P. Duval, and V.Ya. Lipenkov, *Proc. of the NIPR Symp. on Polar Meteorology and Glaciology*, 7, 7 (1993)
43. A.N. Salamatin, V.Ya. Lipenkov, T. Hondoh and T. Ikeda, *Ann. Glaciol.*, 29, in press.

44. T. Ikeda, T. Uchida, and S. Mae, *Proc. of the NIPR Symp. on Polar Meteorology and Glaciology*, 7, 14 (1993)
45. T. Uchida, T. Hondoh, S. Mae, P. Duval, and V.Ya. Lipenkov, *Physics and Chemistry of Ice*, (eds. by N. Maeno and T. Hondoh), Hokkaido Univ. Press, Sapporo, pp. 121 (1992)
46. T. Uchida, T. Hondoh, S. Mae, P. Duval, and V.Ya. Lipenkov, *Ann. Glaciol.*, 20, 143 (1994)
47. T. Hondoh, *Proc. of 2nd Int. Conf. on Natural Gas Hydrates*, 131 (1996)
48. T. Uchida, S. Mae, T. Hondoh, V.Ya. Lipenkov, P. Duval, and J. Kawabata, *Proc. of the NIPR Symp. on Polar Meteorology and Glaciology*, 8, 140 (1994)
49. K. Satoh, T. Uchida, T. Hondoh, and S. Mae, *Proc. of the NIPR Symp. on Polar Meteorology and Glaciology*, 10, 73 (1996)
50. F. Pauer, S. Kipfstuhl, W.F. Kuhs, and H. Shoji, *J. Glaciol.*, 45, 22 (1999)
51. V.Ya. Lipenkov, in preparation
52. H. Craig, H. Shoji, and C.C. Langway, Jr., *Proc. Natl. Acad. Sci. USA*, 90, 11416 (1993)
53. T. Uchida, P. Duval, V.Ya. Lipenkov, T. Hondoh, S. Mae, and H. Shoji, *Mem. Natl. Inst. Polar Res., Spec. Issue*, 49, 298 (1993)
54. E.D. Ershov, and V.S. Yakushev, *Cold Regions Sci. and Tech.*, 20, 147 (1992)
55. H. Shoji and C.C. Langway, Jr., *J. Phys. Chem.*, 87, 4111 (1983)
56. T. Uchida, T. Hondoh, S. Mae, H. Shoji, and N. Azuma, *Mem. Natl. Inst. Polar Res., Spec. Issue*, 49, 306 (1993)
57. *Rika-nenpyo* (Chronological Scientific Tables, ed. Nat. Astronomical Observatory), Maruzen Co. Ltd., Tokyo, pp. 441 (1999) (in Japanese)
58. R.B. Alley, J.H. Perepezko, and C.R. Bentley, *J. Glaciol.*, 32, 415 (1986)